Simulation and PC-based Implementation of a Four Quadrant Direct Torque and Flux Controlled Induction Motor Drive System

A thesis submitted
in partial fulfillment of the requirements
for the degree of

Master of Technology

by

Srinivas Chada

to the

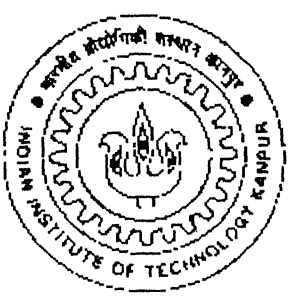

Department of Electrical Engineering
INDIAN INSTITUTE OF TECHNOLOGY, KNPUR

February, 2000

CERTIFICATE

This is to certify that the work contained in this thesis entitled ***Simulation and PC-based Implementation of a Four Quadrant Direct Torque and Flux Controlled Induction Motor Drive System*** by ***Srinivas Chada*** has been carried out under my supervision and that this work has not been submitted elsewhere for a degree.

22.2.2000

Dr. Shyama Prasad Das

Assistant professor,

Department of Electrical Engineering ,

Indian Institute of Technology, Kanpur.

Acknowledgment

I express my deep sense of gratitude and sincere thanks to my thesis supervisor Dr. S. P. Das, for his invaluable active guidance, inspiration and constant encouragement throughout the course of this work. His exemplary patience, concern and understanding has resulted in completion of this work to my fullest satisfaction.

I wish to express my sincere thanks to respected Dr. G. K. Dubey, Dr. A. Joshi, Dr. P. K. Karla, Dr. Sacchidanand, Dr. S. S. Prabhu, and Dr. S. R. Doradla.

I would like to thank my senior colleagues Mr. R. K. Tripati, Ms. Malabika Basu, and Mr. Jamal Jafar for their constant help, support throughout my thesis work. I would also like to thank my batch-mates Murali, S. Gupta, S. P Singh, G.B. Raj, S.P. Pavan, G. S. Rao, T.Murali, Ramakrishna, Surendra, Ullash and my other hall-5 friends for their help and co-operation during my stay at IIT Kanpur. My stay at IITK will remain fresh and evergreen in my memory with the warmth and affection extended by my friends.

I wish to acknowledge the assistance and co-operation rendered by the Power Electronics Lab incharge Mr. O. P. Arora and Mr. Surendra Pal.

Finally I am thankful to my parents and my other family members for their constant encouragement.

Srinivas

ABSTRACT

In the present work the torque and the flux of an induction motor are directly and independently controlled by using "Direct Torque and Flux Control (DTFC)" method. A Synchronous Link Converter (SLC) is used as the front end converter for obtaining unity power factor at all operating conditions at source side including the regenerating modes of the induction motor drive. Thus the drive is capable of operating in all the four quadrants. Hysteresis current control scheme is used to control the synchronous link converter. In DTFC the torque and the flux of the induction motor are controlled by selecting the appropriate voltage vectors from switching logic table which is made with the help of the torque and the flux status. The real time control algorithm of the drive system has been implemented with a PC, which uses ACL-8112PG data acquisition card for data transfer.

Keywords : Synchronous Link Converter (SLC), Direct Torque and Flux Control (DTFC), Data acquisition card, PC .

Contents

List of Figures

List of symbols

σ	leakage factor
γ	Slip angle or torque angle
ω_r, ω_{ref}	Motor actual and reference electrical speed
Ψs , Ψr , Ψs_ref	Stator, rotor and, reference stator fluxes
Ψds , Ψqs , Ψqs , Ψqr	d –axis and q –axis stator and rotor fluxes
C_d	Dc link capacitor
D_1 , D_2 , D_3, D_4	Anti parallel diodes of front end converter
dT, dΨ	Torque and flux stator flux
f_ds , f_qs , f_dr, f_qr	Motor stator and rotor d -axis and q –axis fluxes in the control program
flux_s, flux_ref	Stator actual flux and reference flux in control program
I_a,I_b,I_c	Motor phase currents
I_d	Dc link current
I_{dc}	Inverter current
i_{ds} , i_{qs} , i_{dr} , i_{qr}	d–axis and q–axis stator and rotor currents
I_l	Load current in control program
I_{rms}	RMS current
I_s	Source current
I_{s_ref}	Reference source current
I_{s1}	Fundamental component of the source current
J	Moment of inertia
K_p,K_i , K_{pr},K_{ir}	PI controller gain constants

L_s, L_r ,M	Stator and rotor and magnetizing inductances
L_{sr}	Synchronous link inductor
P	Number of induction motor poles
R_s	Synchronous link inductor resistance
S_1,S_2,S_3,S_4 ,	Converter switches of the front end converter
S_a, S_b, S_c	Switching statuses of inverter
sw	Switching status of synchronous link converter
T_e, T_l, T_{e_ref}	Electromagnetic ,load and reference torque
V_a , V_b , V_c	Induction motor phase voltages
V_{ao},V_{bo},V_{co}	Voltage outputted by inverter
V_{dc}	Dc link voltage
V_{ds} , V_{qs}	d -axis and q –axis flux
V_s	Source voltage
x	% of ripple in dc link voltage

Chapter 1

INTRODUCTION

1.1 Background

Adjustable speed drives are widely used in industries. The de-facto industrial standard necessitates the drives to have fast torque and speed response, four quadrant operation capability, high torque-to-weight ratio in addition to overall economy. Furthermore, with the increased concern about power quality issues, an ideal industrial drive should draw sinusoidal input current at unity power factor from the utility.

Traditionally, separately excited dc machines were the obvious choice for applications in adjustable speed drives, where independent torque and flux control is required. In dc machine, the torque can be controlled over a wide range of speed by independent variation of field current and armature current. The dc machines also have the excellent dynamic performance over wide range of operating conditions due to inherent decoupling between field flux and armature current. On the other hand, dc machines are inherently bulky, require frequent maintenance, have low torque-to-weight ratio, in addition to having commutation problems. In comparison to dc machines, induction motors are robust, less expensive, and have high torque-to-weight ratio. But from electrical point of view, induction motor is a single excited machine. Thus the control of torque and flux in induction motor is not as simple as that in the case of a dc motor due to non linear interaction between torque and flux in the former, giving rise to oscillatory dynamic response.

Constant voltage/ hertz control is one of the popular methods for speed control of induction motor. This aims at maintaining the same terminal voltage to frequency ratio so as to give a nearly constant flux over wide range of speed variation. In this control scheme, the performance of the machine improves in the steady state only, but the transient response is poor. Moreover constant voltage/hertz control keeps the total stator flux linkage constant in steady state without maintaining decoupling between the flux and the torque.

In 1971, Blaschke [8] proposed a scheme, which aims as the control of an induction motor like a separately excited dc motor, called field oriented control, vector control, or transvector control. In this scheme, the induction machine is analysed from a synchronously rotating reference frame where all fundamental ac variables appear to be dc ones. The torque and the flux component of currents are identified and controlled independently to achieve a good dynamic response. However, there is a necessity of transforming the variables in the synchronously rotating reference frame to the stator reference frame to effect the control of actual currents / voltages. This transformation contains transcendental functions like sine, cosine, and also introduces computational complexity into the system. Additionally, the transformation also needs the appropriate flux vector angle, which is either calculated by adding the calculated slip angle and measured rotor angle as in indirect vector control [9 , 15], or by estimating the flux angle flux angle directly by employing a flux observer as in direct vector control. Thus the accuracy of the vector control is largely governed by the accuracy with which flux angle is calculated and the rotating reference frame variables are transformed into the stator variables.

Recently advanced control strategies for PWM inverter-fed induction motor drives have been developed based on the space vector approach, where the torque and flux of an induction motor can be directly and independently controlled without any co-ordination transformation. One of the emerging methods, in this perspective is the *Direct Torque and Flux Control* (DTFC) method [11, 12, 14]. In DTFC, the motor torque and the flux are calculated from the primary variables, and they are controlled directly and independently by selecting optimum inverter switch modes. This selection is made so as to restrict the errors

of flux and torque within the hysteresis bands. This control results in quick torque response in the transient operation and improvement in the steady state efficiency.

In inverter-fed induction motor drives, a dc power source is required to feed the dc link. Traditionally, the power conversion from *ac to dc* was achieved by uncontrolled diode rectifiers or thyristorised controlled converters. Such converters have drawbacks such as harmonics in the input current, and output dc voltage, in addition to low input power factor for thyristor controlled converters particularly at low output voltages. Furthermore, four quadrant operation is not possible without employing a dual converter. Several induction motor drive applications require the front end *ac to dc* converter to have both rectifying and regenerating abilities. Dual converter used under such requirements has complexity in power and control circuits. The Synchronous Link Converter(SLC) can be used as a front end converter [1-5] to reduce the harmonics in the line current, and to get the unity power factor. Additionally, reversible power flow can also be achieved using an SLC.

1. 2 Objectives of the Thesis

The objectives of the present work is to realize a variable speed induction motor drive where the torque and the flux of an induction motor is controlled directly and independently by using *Direct Torque and Flux Control*(DTFC) method [11, 12, 14]. At the same time, the unity power factor is maintained by using a single phase SLC as the front end *ac* to *dc* converter. The dc link voltage is regulated by a closed-loop feedback using a PI controller. Unity power factor is obtained by controlling front end converter switches in such a way that the source current follows the reference current which is in phase with the source voltage.

The present thesis deals with the design, digital computer simulation and PC-based implementation of a four quadrant direct torque and flux controlled induction motor drive system.

1.4 Summary of the Chapters

Chapter 2 describes the basic operation of a single phase Synchronous Link Converter. Modeling and digital computer simulation has been made with resistive load. Simulation results are presented at the end of the chapter.

Chapter 3 highlights the digital computer simulation of the proposed four quadrant DTFC of induction motor. Mathematical modeling of the DTFC is presented. Digital computer simulation has been made with the Synchronous Link Converter used as the front end converter. Typical simulation results are presented at the end of the chapter.

Chapter 4 describes the PC-based implementation of control scheme using a high performance data acquisition card for purpose of the data transfer. Brief discussions about the power circuit and the control circuit are given with requisite diagrams.

In chapter 5 experimental and simulation results are compared with the help of waveforms.

Chapter 6 enumerates the main contributions of the present thesis and suggests the scope for future work.

Chapter 2

MODELING AND SIMULATION OF SYNCHRONOUS LINK CONVERTER

2.1 Introduction

The power conversion from *ac* to *dc* has been traditionally dominated by uncontrolled rectifiers or phase controlled converters. Such converters have the inherent draw backs such as, harmonics in the input current and output dc voltage, in addition to low input power factor particularly at low output voltages. Variable speed drive applications require *ac* to *dc* converters to have both rectifying and regenerating abilities. Dual converters can be used under such requirements, but they have complex power and control circuits. The Synchronous Link Converters(SLC) can be used as front end converter under such applications with rectifying and regenerating abilities.

Synchronous Link Converters have several advantages such as sinusoidal input currents, unity input power factor, inherent regenerative capability and these make SLC a plausible choice for *ac* to *dc* converter in a variable speed drive applications. This chapter deals with the modeling and simulation of a single phase Synchronous Link Converter.

2.2 Basic Single Phase Synchronous Link Converter

2.2.1 Principle of a synchronous link converter

The power circuit configuration for the single phase is shown in Fig. 2.1. It is operated in controlled current boost type converter mode [2, 3, 4]. The source current (I_s) is made to follow a sinusoidal reference current within a hysteresis band. The hysteresis band width determines the source current profile, its harmonic spectrum and the switching frequency of the devices. From the Fig. 2.1 the source current (I_s) can be increased by turning on the S_2, S_3, and source current can be decreased by turning on the S_1, S_4. The dc link capacitor voltage is kept constant throughout the operation.

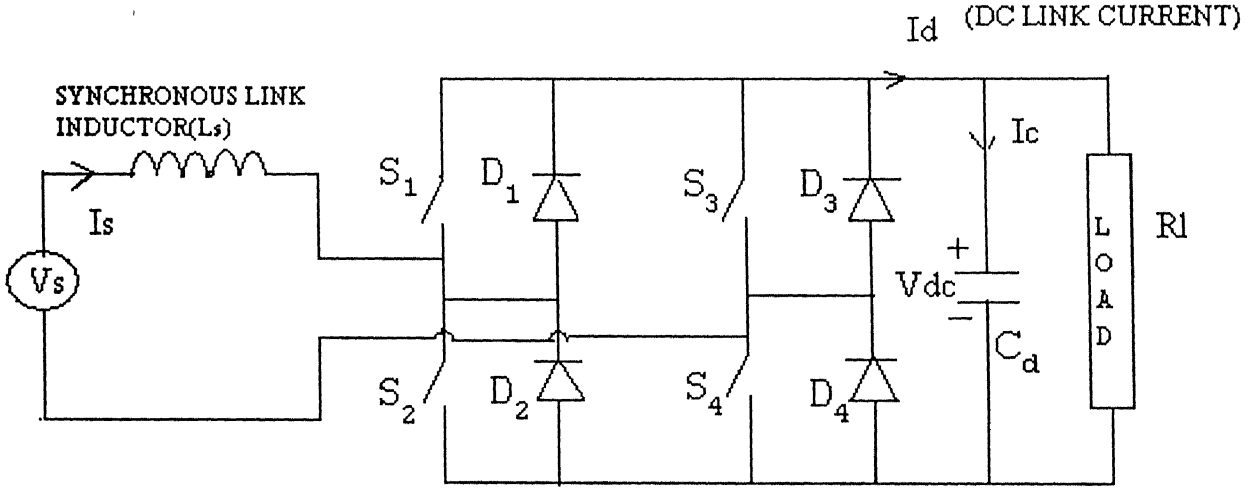

Fig. 2.1 Basic single phase synchronous link converter

The switching logic employing hysteresis current control can be written as follows.

If $I_s \geq I_{s\,ref} + \Delta I$ then switches S_1, S_4 turn on.

If $I_s < I_{s\_ref} - \Delta I$ then switches S_2, S_3 turn on.

Where ΔI is the hysteresis band on the reference current.

The dc voltage rating of the capacitor will depend upon the dc link voltage. It is necessary to have a safety factor of 1.25 for the rated voltage of the capacitor over the actual dc link voltage to account for over charging during transients.

2.2 Hysteresis Current Controlled Scheme

The hysteresis current controlled scheme block diagram as shown in Fig. 2.2. The dc link voltage is compared with the reference dc link voltage command to control the amplitude of the reference current . The error between the actual dc link voltage and reference dc link voltage is processed through a PI controller, which gives the amplitude of the source current. The source current amplitude is multiplied by sin(wt) which is in phase with the ac voltage to generate reference source current to the converter. Then control of the switches S_1, S_2, S_3, and S_4 is made in such a way that the source current follows the reference current. The dc link voltage remains constant at all the zero crossing instants of the source voltage. So the dc link voltage is sensed at these instants to eliminate second harmonics in the source current.

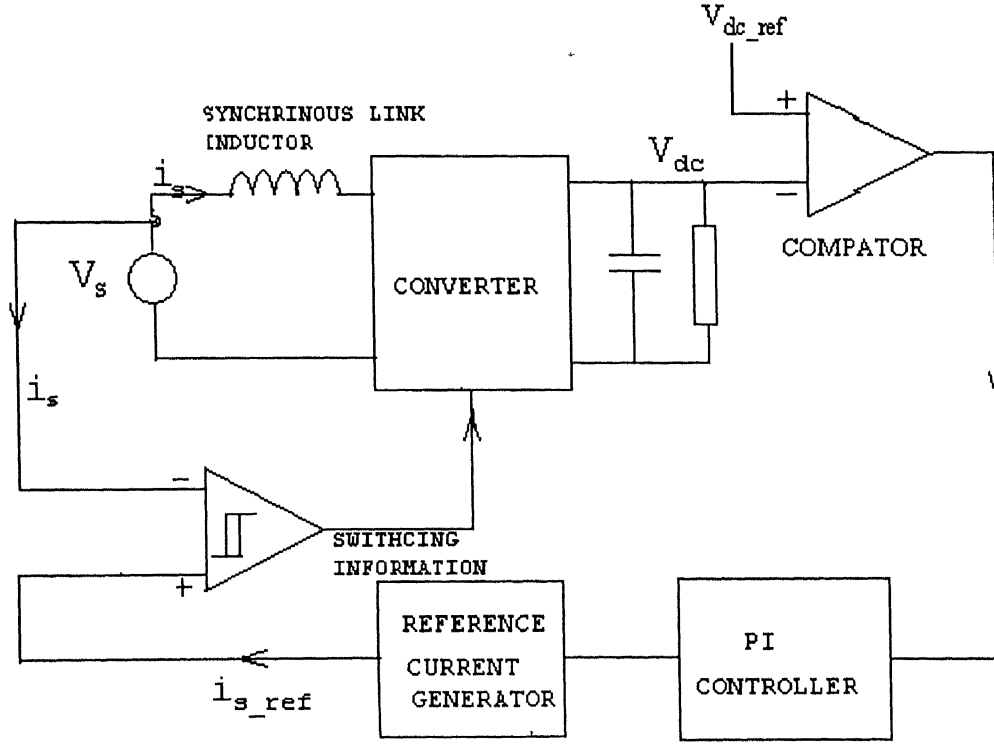

Fig 2 2 Hysteresis current controlled scheme for SLC

3.2 Basic Concept of DTFC

By using the instantaneous vectors, the dynamic behavior of induction machine can be expressed not only in the steady state but also in transient state. In general the torque the expression of an induction motor is (Fig. 3.1) given by

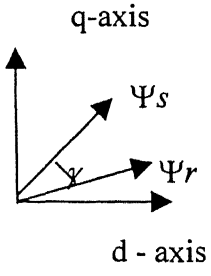

Fig. 3.1

$$Te = \frac{3}{2} * \frac{P}{2} \frac{M}{\sigma LsLr} |\Psi s||\Psi r| \ sin(\gamma) \qquad (3.1)$$

Ψs ---------- stator flux

Ψr ---------- rotor flux

γ ---------- angle between the stator flux and stator flux (torque angle)

$\sigma = 1 - \frac{M^2}{LsLr}$ --------- leakage factor

The stator flux is the state variable which can be adjusted by stator voltage. In the space vector PWM inverter, the stator voltage vector is

$$V_s = \sqrt{2/3}\ [V_a + V_b \exp(j2\pi/3) + V_c \exp(j4\pi/3] \qquad (3.2)$$

where V_a, V_b, V_c instantaneous values of primary line-to-neutral voltages and are determine by the switching modes of inverter as shown in Fig. 3.2

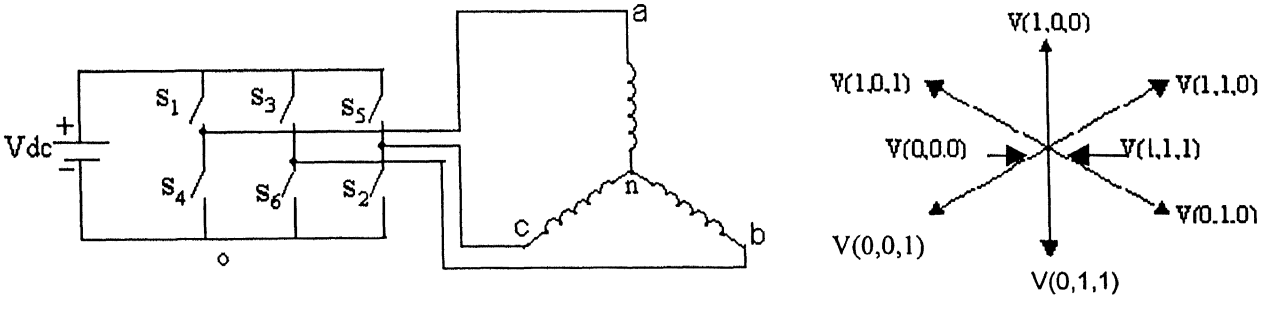

Fig. 3.2 Schematic diagram of PWM inverter and instantaneous voltage vectors

The switching logic for the current controlled scheme is given by

If $I_s \geq I_{s\_ref} + \Delta I$ then switches S_1, S_4 turn on.

If $I_s < I_{s\_ref} - \Delta I$ then switches S_2, S_3 turn on.

2.4 Digital Simulation

Fig. 2.3 and Fig 2.4 show the different states, in the operation of the Synchronous Link Converter during positive half cycle of supply voltage. For decreasing the source current, switches, S_1, S_4 are turned on. In this state, if the source current is positive, anti-parallel diodes, D_1, D_4, conduct as shown in Fig. 2.3a. If the current is negative, the switches, S_1, S_4, conduct as shown in Fig. 2.3b.

For increasing the source current switches, S_2, S_3 are turned on. In this state, if the source current is positive, the switches, S_2, S_3, conduct as shown in Fig. 2.4a. If the source current is negative, the anti-parallel diodes, D_2, D_3, conduct shown as in Fig. 2.4b.

From Fig. 2.3, when the switches S_1, S_4 conduct the equations are

$$V_s = L_{sr}\frac{dI_s}{dt} + R_s * I_s + V_{dc} \qquad (2.1)$$

$$I_d = C_d\frac{dV_{dc}}{dt} + I_l \qquad (2.2)$$

The dc link current I_d is given by

$$I_d = I_s \qquad (2.3)$$

$$I_s = C_d\frac{dV_{dc}}{dt} + I_l \qquad (2.4)$$

The load current I_l is given by

$$I_l = \frac{V_{dc}}{R_l} \qquad (2.5)$$

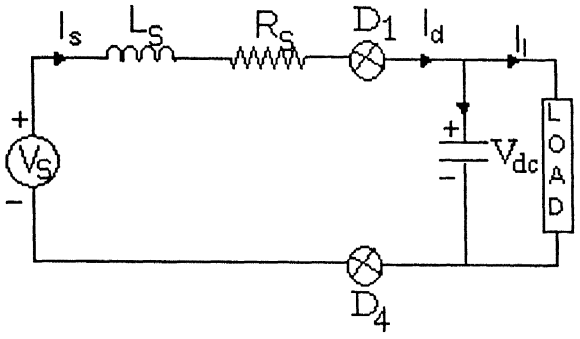

Fig. 2 3a

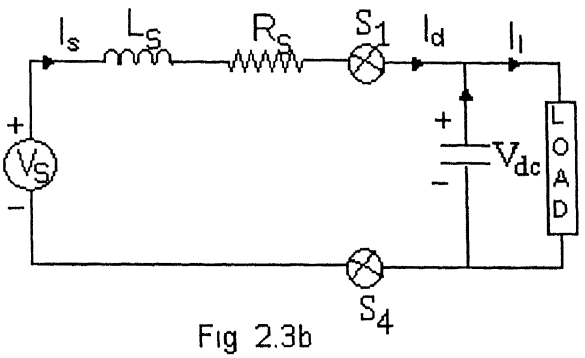

Fig 2.3b

Fig. 2.3 Different states in the operation of synchronous link converter for decreasing the current

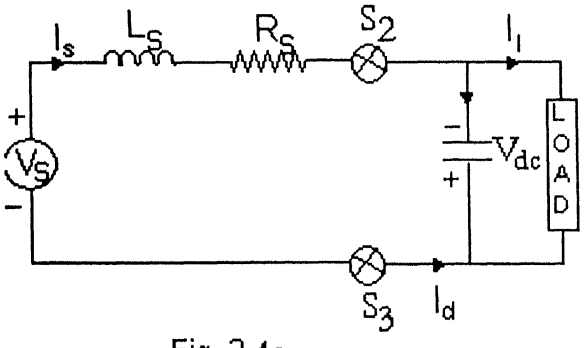

Fig 2 4a

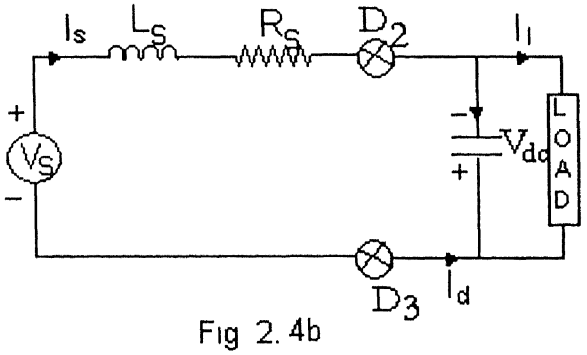

Fig 2. 4b

Fig. 2. 4 Different states in the operation of synchronous link converter for increasing the current

From the above equations (2.1 - 2.5)

$$\frac{dI_s}{dt} = \frac{V_s - R_s * I_s - V_{dc}}{L_{sr}} \tag{2.6}$$

$$\frac{dV_{dc}}{dt} = \frac{I_s - V_{dc} / R_l}{C_s} \tag{2.7}$$

The equations (2.6) and (2.7) suggest that the slope of I_s is negative for $V_{dc} > V_s$. Hence the source current I_s decreases, and the capacitor charges and dc link voltage increases.

In the Fig. 2.4, when the switches, *S2, S3,* conduct the equations are,

$$V_s = L_{sr} \frac{dI_s}{dt} + R_s * I_s - V_{dc} \tag{2.8}$$

$$I_d = -C_d \frac{dV_{dc}}{dt} + I_s \tag{2.9}$$

The dc link current I_d is given by

$$I_d = -I_s \tag{2.10}$$

From above equations (2.8 - 2.10)

$$\frac{dI_s}{dt} = \frac{V_s + V_{dc} - R_s * I_s}{L_{sr}} \tag{2.11}$$

$$\frac{dV_{dc}}{dt} = \frac{-I_s - V_{dc} / R_l}{C_d} \tag{2.12}$$

The equations (2.11) and (2.12) suggest that the slope of I_s is positive. Hence the source current increases, during this interval. The capacitor discharges, the dc link voltage decreases.

In general, the equations (2.6), (2.7), (2.11), and (2.12) can be written in matrix form as follows

$$\frac{d}{dt}\begin{bmatrix} I_s \\ V_{dc} \end{bmatrix} = \begin{bmatrix} \frac{-R_s}{L_{sr}} & -sw\frac{1}{L_{sr}} \\ sw\frac{1}{C_d} & \frac{1}{C_d R_l} \end{bmatrix} \begin{bmatrix} I_s \\ V_{dc} \end{bmatrix} + \begin{bmatrix} V_s \\ 0 \end{bmatrix} \tag{2.13}$$

where ,

sw is the switching function

if $S1, S4$ conducts $sw=1$,

if $S2, S3$ conduct $sw=-1$

The equation (2.13) can be solved by R-K fourth order method and the values of V_{dc}, I_s can be obtained. A computer program was developed for resistive load. The data for simulation are given below,

1. Input supply voltage V_s=40V 1ϕ , 50Hz.
2. Output dc voltage V_{dc}=100V
3. Output voltage ripple = 5% of V_{dc}
4. Synchronous link inductor(L_{sr})= 8mH.
5. DC capacitor C_d=2000 μF
6. Load resistance R_l = 100 Ω

In the simulated results, the input current waveform, the source voltage, the dc link voltage and the harmonic spectrum of the source current are shown in Fig. 2.5, Fig. 2.6, and Fig. 2.7 respectively. Fig 2.5 shows that the input source current (I_s) is in

phase with source voltage. Fig 2.6 shows that the dc link voltage is nearly constant during the operation. In Fig. 2.7, the harmonic spectrum of source current is shown. The magnitude of low order harmonics is low. Higher order harmonics can be eliminated by using filters.

2.5 Conclusions

Due to advantages like reduced line current harmonics, unity power factor operation and bi-directional power flow capability, synchronous link converters are widely used as front end converters in regenerative ac drives. Hysteresis current controlled scheme is used, and unity power factor operation is shown in simulation results.

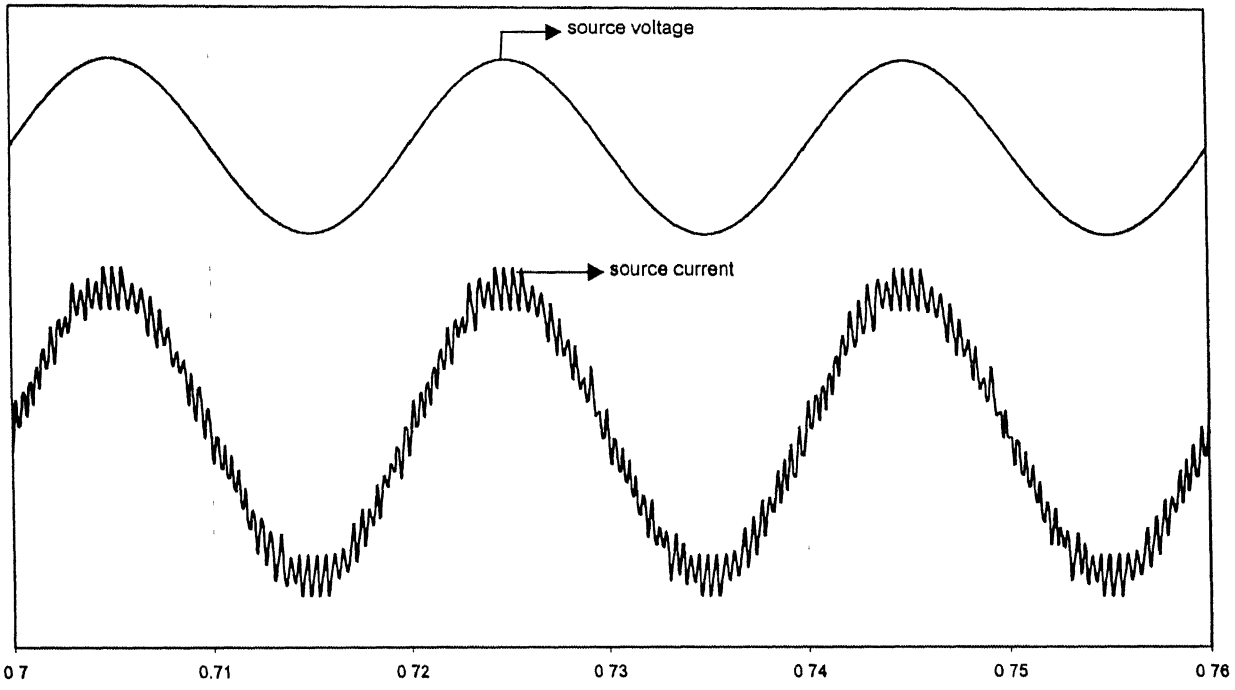

x axis 1 div = .01s (time)
y axis 1 div = 40V (soyrce voltage)
y axis 1 div = 2 amps (source current)

Fig. 2.5 Source voltage and source current

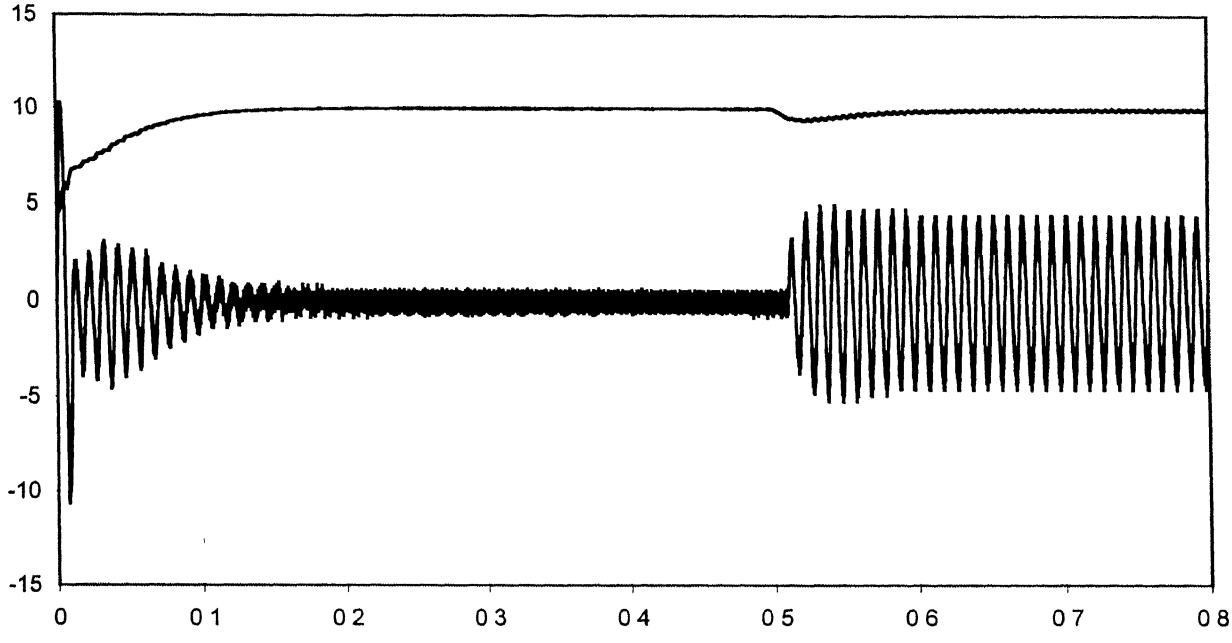

x axis 1 div = .2 sec (time)
y axis 1 div = 10 volts (dc link voltage)

Fig. 2.6 Dc link voltage waveform load is applied at 0 5 s

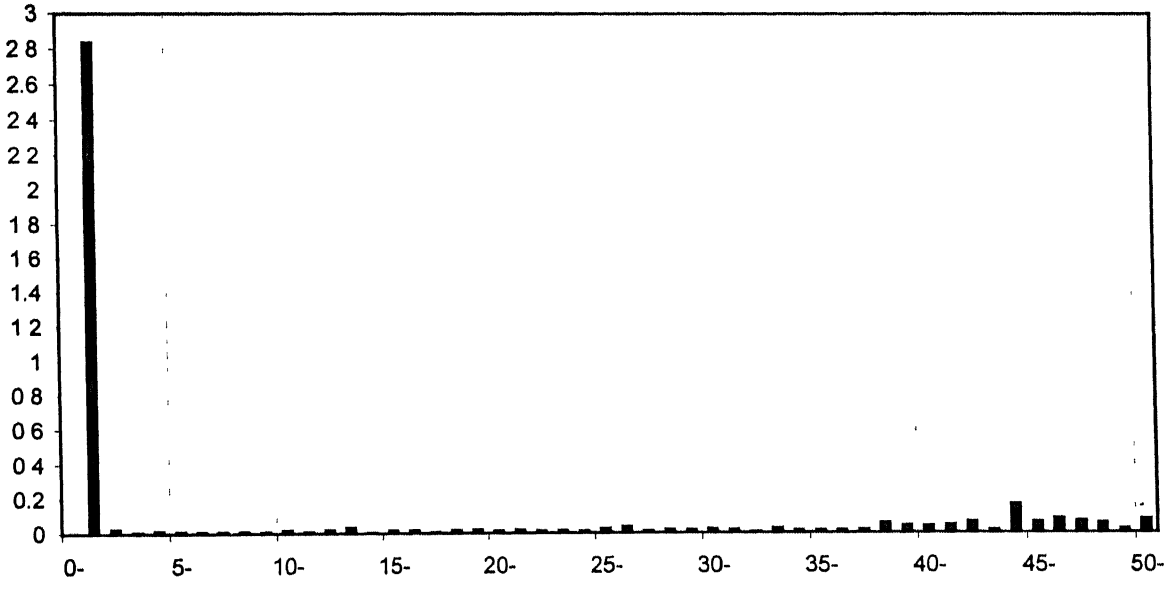

y axis 1 div = 5 (harmonic number)
x axis 1 div = .5 (hormonic magnitudes)

Fig 2.7 Supply current harmonic spectrum

Chapter 3

MODELING AND SIMULATION OF THE PROPOSED INDUCTION MOTOR DRIVE

3.1 Introduction

With the recent progress in power semiconductor device technology followed by advancement in electronic control methods, variable speed inverter-fed ac motor drives are used in variety of applications. In Field Oriented Control (FOC), induction motors have high dynamic and static performance like dc motor drives. But FOC scheme requires coordinate transformation. On the other hand, Direct Torque and Flux Control (DTFC) of induction motor requires no coordinate transformation of variables. The torque and the stator flux can be controlled directly and independently by selecting the optimum space voltage vectors, within hysteresis bands.

Variables speed induction motor drives need regenerative braking capability. If diode rectifiers or phase controlled rectifiers are used as a front end converter, regenerative braking is not possible. In addition, for these converters source current has harmonics, and the power factor is less then unity. The above problems are overcome by using the Synchronous Link Converter as the front end converter. The present chapter is devoted to the development of control schemes and digital simulation of direct torque and flux control of induction motor with current controlled synchronous link converter used as a front end ac to dc converter. The induction motor is simulated in the stationary reference frame. Typical simulation results are given at the end of this chapter

Considering the combinations of status of switches S_a, S_b, S_c, the inverter has eight conduction modes. By using the switching functions S_a, S_b, S_c (whose values are either 1 or 0), the voltage can be expressed as

$$V_s(S_a, S_b, S_c) = \sqrt{2/3}\ V_{dc}(S_a + S_b \exp(j2\pi/3) + S_c \exp(j4\pi/3)) \qquad (3.3)$$

Here, V_{dc} is dc link voltage of the inverter. While in operation, the inverter output voltage can be one of two states, either a active vector (one of the six non zero vectors V_s (001), to $V_s(110)$), or a zero vector (one of the zero vectors $V_s(000)$, $V_s(111)$). From [14], the flux linkage vector Ψs is expressed by integral of voltage vector.

$$\Psi s = \int (V_s - i_s r_s)\, dt \qquad (3.4)$$

Considering the resistance of the winding to be small, the trajectory of Ψs moves in the direction of the inverter output voltage vector [14]. When the output is one of nonzero voltage vectors, Ψs moves at constant velocity which is proportional to the output voltage. In the case of a zero voltage vector, the stator flux velocity is small and can be considered to be zero because of small value of resistive drop. This shows if proper selection of the voltage vectors is made, the trajectory of Ψs can follow a specified path. By selecting the proper voltage vectors, the magnitude of Ψs can be kept constant, and the rotating velocity of Ψs can be controlled by changing the output voltage ratio between zero voltage vectors and active voltage vectors. The torque angle (γ) and Ψs are directly related with the torque and efficiency . If the amplitude and rotating velocity of Ψs is changed freely, both the torque and the flux control can be achieved at a time.

Fig. 3.11 shows that the torque and flux can be independently controlled. By applying the load at 0.5s there no change is observed in flux and speed. Also, by changing the flux from 0.56 wb to 0.4 wb, no change is found in torque and speed. Fig. 3.12 shows the motor phase currents. Fig. 3.13 shows the plot between the d – axis and q – axis stator fluxes . It follows that the stator flux is nearly sinusoidal. Fig. 3.14 gives the d - axis and q -axis flux profiles under normal operating conditions.

Fig. 3.15 shows the dc link voltage and speed profiles. The speed reference is changed from 500 rpm to –500rpm at 1s. The actual speed changes from 500rpm to -500rpm within 0.3sec. During the speed reversal induction motor goes through regenerative mode. During the regenerative mode the power is fed from motor side to ac source side. Ac source voltage and source currents are in out of phase during regenerative mode shown in Fig. 3.16. The dc link voltage also increase momentarily as shown in Fig 3.15. Fig. 3.18 shows the forward motoring, forward braking, reverse motoring, and reverse braking capability of the drive system. Hence the drive is found to have four quadrant capability.

3.11 Conclusions

The analysis of the four quadrant direct torque and flux control of induction motor has been made in this chapter. Synchronous link converter is used as the front end converter for bi-directional power flow and to get unity power factor at the source side. The machine parameters are assumed to be constant at all operating conditions. The drive is found to have four quadrant capability. The rate of change of torque depends upon the time differential of the slip angle. Hysteresis current controlled scheme is used for the synchronous link converter.

3.3 Control of Flux

Selection of V_s (S_a, S_b, S_c) is made so that the error between the stator flux $|\Psi s|$ and the reference stator flux $|\Psi s\_ref|$ lies between the limit $\pm \Delta\Psi s$. This selection depends upon the magnitude of Ψs, as well as the direction of rotation. As depicted in Fig. 3.2, the inverter voltage vectors change periodically by a step of $\pi/3$ radians. Hence, for discrimination, the dq-plane is divided into six sectors and depending upon the direction of rotation (clockwise or anti-clockwise) the requisite voltage vector is picked. This is shown in Fig 3.3. If clockwise rotation of the stator flux vector Ψs is considered then the switching logic is selected such that the

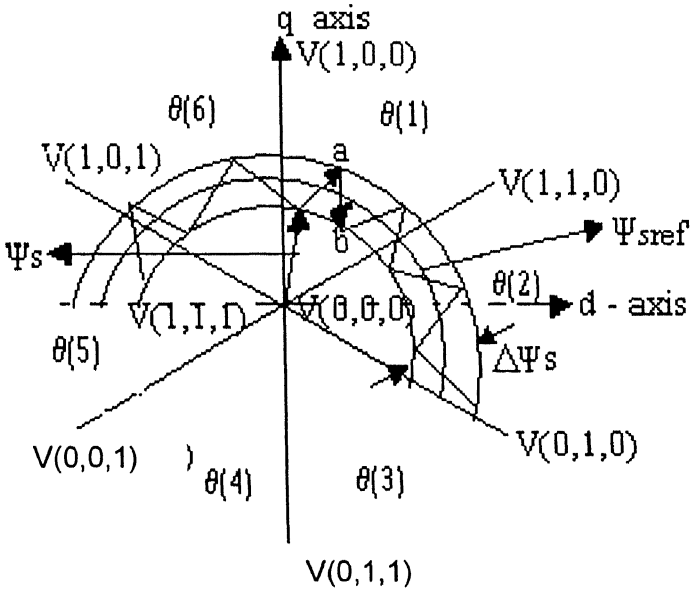

Fig. 3.3 Selection of voltage vectors for flux control

magnitude of the flux is lies within the hysteresis band. This can be explained with the help of Fig. 3.2 and Fig 3.3. The flux is in the sector 1 in Fig 3.3. For a clockwise rotation, either voltage vector V (1,1,0) or vector V (0,1,0) should be selected. When the flux touches the upper limit ($|\Psi s| + \Delta\Psi s/2$) of the hysteresis band (point 'a' in Fig. 3.3) vector V(0,1,0) must be chosen. When the flux touches the lower limit ($|\Psi s| - \Delta\Psi s/2$) (point 'b'), vector V(1,1,0) should be selected. If eq. (3.3) and eq. (3.4) are combined, the expression for stator flux can be written as

$$\Psi s = \sqrt{2/3}\, V_{dc}[S_a+S_b\exp(j2\pi/3) +S_c\exp(j4\pi/3)].\ \Delta t + \Psi s_0 \quad (3.5)$$

where Ψs_0 is the initial value of flux. For the voltage vector of V(0,1,0)

$$\Psi s = \sqrt{2/3}\, V_{dc}.\ \exp(j2\pi/3)\ .\ \Delta t + \Psi s_o \quad (3.6)$$

$$= \sqrt{2/3}\, V_{dc}(-1/2 + j\ \sqrt{3/2}\ )\ \Delta t + \Psi dso - j\ \Psi qso \quad (3.7)$$

The above equation shows that new value of Ψds and Ψqs have reduced. Also the flux vector rotates in the clockwise direction. The same idea can be extended to understand the counter-clockwise rotation of the flux vector. This also establishes that the magnitude and direction of rotation of the flux vector is dependent upon selection of the space voltage vectors.

3.4 Torque Control

Under constant Ψs control, the rate of increasing of torque is almost proportional to time differential of the flux angle γ (i.e. torque angle). The time differential of flux angle is nothing but slip speed. When the actual torque T_e is less then reference torque (T_{e_ref}), it is necessary to increase T_e as fast as possible by applying a suitable voltage vector. This means the accelerating vector which possesses maximum rate change of flux angle ($\frac{d\gamma}{dt}$) should be selected. When T_e is equal to T_{e_ref} it is required to decrease T_e as slowly as possible. The slowest degenerative operation can be obtained by using zero voltage vector. The selection of V_s (S_a, S_b, S_c) is made such that T_e remains within the band.

3.5 Switching Logic Selection Table

Depending upon the status of error of $|\Psi s|$ and T_e, a switching table can be constructed. The status of the error of the $|\Psi s|$ and T_e can be detected and digitized by simple two and three level hysteresis comparators respectively.

The digitized output signals of the flux controller are defined as

If $\Psi s \leq \Psi s\_ref - \Delta\Psi s$ then $d\Psi = 1$

If $\Psi s \geq \Psi s\_ref + \Delta\Psi s$ then $d\Psi = 0$

And those of the torque controller are defined as

If $T_e < T_{e\_ref} - \Delta T_e$ then dT=1

If $Te > T_{e\_ref} + \Delta T_e$ then dT=-1

If $(T_e - \Delta T_e) < T_e < (T_e + \Delta T_e)$ then dT=0

The optimum switching table, thus obtained, is shown in Fig 3.4.

		Θ(1)	Θ(2)	Θ(3)	Θ(4)	Θ(5)	Θ(6)
dψ=0	dT=1	V(1,1,0)	V(0,1,0)	V(0,1,1)	V(0,0,1)	V(1,0,1)	V(1,0,0)
	dT=0	V(1,1,1)	V(0,0,0)	V(1,1,1)	V(0,0,0)	V(1,1,1)	V(0,0,0)
	dT=-1	V(1,0,1)	V(1,0,0)	V(1,1,0)	V(0,1,0)	V(0,1,1)	V(0,0,1)
dψ=1	dT=1	V(0,1,0)	V(0,1,1)	V(0,0,1)	V(1,0,1)	V(1,0,0)	V(1,1,0)
	dT=0	V(0,0,0)	V(1,1,1)	V(0,0,0)	V(1,1,1)	V(0,0,0)	V(1,1,1)
	dT=-1	V(0,0,1)	V(1,0,1)	V(1,0,0)	V(1,1,0)	V(0,1,0)	V(0,1,1)

Fig. 3.4 Optimum switching table

3.6 Simulation of Induction Motor

For simulation of induction motor, the motor is analyzed in stationary reference frame. The motor is fed from the voltage source inverter as shown in Fig. 3.5. For a given set of switching information, V_{ao}, V_{bo}, V_{co} have discrete instantaneous values

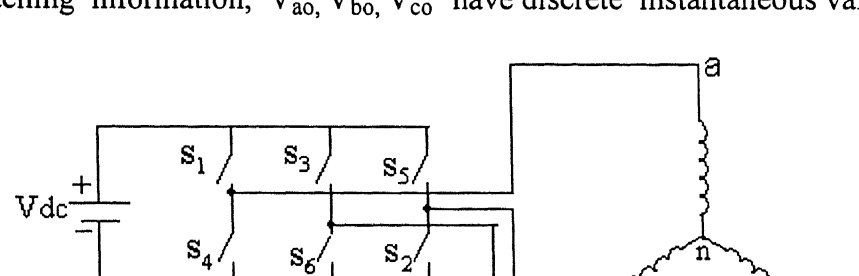

Fig. 3.5 Schematic diagram of PWM inverter

$V_{ao} = V_{dc}$ if S_1 is on, S_4 is off

$= 0$ if S_1 is off, S_4 is on

The same logic applicable for V_{bo} and V_{co}

Thus

$$V_{an} = (1/3)(2*V_{ao} - V_{bo} - V_{co}) \quad (3.8)$$

$$V_{bn} = (1/3)(2*V_{bo} - V_{co} - V_{ao}) \quad (3.9)$$

$$V_{cn} = (1/3)(2*V_{co} - V_{ao} - V_{bo}) \quad (3.10)$$

Transformation of ac voltages from a, b, c (3-phase) frame to d, q (2-phase) stationary reference frame gives

$$V_{ds} = (2/3)(V_{an} - .5(V_{bn} + V_{cn})) \quad (3.11)$$

$$V_{qs} = (2/3)(V_{bn} - V_{cn})(.866) \quad (3.12)$$

Now,

$$V_{ds} = i_{ds} r_s + p\Psi_{ds} \quad (3.13)$$

$$V_{qs} = i_{qs} r_s + p\Psi_{qs} \quad (3.14)$$

$$0 = i_{dr} r_r + p\Psi dr + \omega_r \Psi qr \quad (3.15)$$

$$0 = i_{qr} r_r + p\Psi qr - \omega_r \Psi dr \quad (3.16)$$

$$\text{Also } \Psi ds = L_s i_{ds} + M i_{dr} \quad (3.17)$$

$$\Psi qs = L_s i_{qr} + M i_{qr} \quad (3.18)$$

$$\Psi dr = L_r i_{dr} + M i_{ds} \quad (3.19)$$

$$\Psi qr = L_r i_{qr} + M i_{qs} \quad (3.20)$$

The equation 3.13 - 3.16 can be written in the matrix form as follows.

$$\begin{pmatrix} V_{ds} \\ V_{qs} \\ 0 \\ 0 \end{pmatrix} = \begin{pmatrix} r_s + L_s p & 0 & Mp & 0 \\ 0 & r_s + L_s p & 0 & Mp \\ Mp & M\omega_r & r_r + pL_r & L_r\omega_r \\ -M\omega_r & Mp & -L_r\omega_r & r_r + pL_r \end{pmatrix} \begin{pmatrix} i_{ds} \\ i_{qs} \\ i_{dr} \\ i_{qr} \end{pmatrix} \quad (3.21)$$

These above set of differential equations can be solved by R – K fourth order method and the values of i_{ds}, i_{qs}, I_{dr}, and I_{qr} can be obtained. The stator fluxes in d- axis and q- axis can be found out from equation 3.17 and 3.18. The electromagnetic torque expression is given by

$$Te = (3/2)(P/2)\,(\Psi ds\ i_{qs} - \Psi qs\ i_{ds}) \quad (3.22)$$

and the stator flux is given by

$$\Psi s = \sqrt{\Psi ds * \Psi ds + \Psi qs * \Psi qs} \quad (3.23)$$

The speed of rotor in electrical rad/sec is

$$\omega_r = (P/2)(1/J)(T_e - T_l - B(2/P)\omega_{ro})$$

The reference torque T_{e_ref} is generated by speed error processed through the PI controller. The output of PI controller is given as follows

$$T_{e\_ref}(n) = T_{e\_ref}(n\_1) + K_p(error(n)-error(n\_1)) + K_i\, error(n\_1)\,\Delta t \quad (3.24)$$

The actual values of the electromagnetic torque T_e and actual flux Ψs are compared with the reference torque Te_ref and reference flux Ψs_ref. The optimum voltage vector $V_s(S_a, S_b, S_c)$ can be obtained by using the torque and flux status.

3.7 Application of Synchronous Link Converter in DTFC of Induction motor

The analysis and simulation of the synchronous link converter with resistive load has been discussed in chapter 2. When the synchronous link converter used as the front end converter in induction motor drive system, the power balance equation of the system is given as follows.

inverter input = motor input (by neglecting the converter losses)

= rotor input + stator losses

$$V_{dc}*I_{dc} = T_e*\omega_r + 3/2*I_{rms}*I_{rms}*R_s \quad (3.25)$$

where ω_r is the motor speed, and Te is electromagnetic torque developed by induction motor as given by equation (3.22).

The load current for the synchronous link converter is given by

$$I_{dc} = (T_e * \omega_r + 3/2*I_{rms}*I_{rms}*R_s)/V_{dc} \quad (3.26)$$

In the motoring mode the inverter input current I_{dc} positive, i.e. the power flow is from the source to the motor. In the regenerating mode current I_{dc} is negative i.e. the

induction motor acts as a generator and the power is fed from the motor to the source. During this period source current and source voltage are out of phase (180^0) as shown in the simulation results.

3.8 PI Controller Simulation

The basic block diagram of pi controller as shown in Fig. 3.6

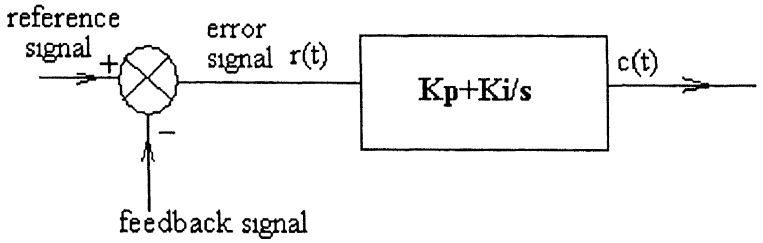

Fig 3 6 PI controller

In continuous time domain a PI controller output represented by following equation

$$c(t) = K_p r(t) + K_i \int_0^t r(t) \tag{3.27}$$

The reference torque is generated by speed error processed through the PI controller

$$T_{e\_ref} = K_p\, e(t) + K_i \int_0^t e(t) \tag{3.28}$$

where $e(t) = \omega_{ref} - \omega_r$

In a digital computer system, the speed sampling is in discrete time, and so a discrete time model is desired. Taking the sampling interval to be Δt

$$T_{e\_ref}(n) = T_{e\_ref}(n\_1) + K_p\,(e_{sn} - e_{s(n\_1)}) + K_i\, e_{s(n\_1)}\,\Delta t \tag{3.29}$$

Similarly, the reference source current is generated by the dc link voltage error which is processed through another PI controller

$$I_{s\_ref}(n) = I_{s\_ref}(n\_1) + K_{pr}\,(e_{dcn} - e_{dc(n\_1)}) + K_{ir}\,e_{dc(n\_1)}\,\Delta t \qquad (3.30)$$

3.9 Block Diagram for Four Quadrant DTFC

To visualize the different steps of the simulation, a block diagram has been drawn as shown in Fig. 3.7. The source current reference is obtained by the dc link voltage error processed through a PI controller. The torque reference is obtained by the speed error processed through the speed PI controller. The motor model block takes the three phase motor currents, the switching status of the inverter, the dc link voltage, and calculates the stator flux and the torque. These variables are compared with the reference values to give the torque and the flux status. The appropriate voltage vectors are selected based on the torque and the flux status from the table shown in the Fig. 3.4.

3.10 Simulation Results

The flow chart of the computer simulation is shown in Fig. 3.8, and the program listing in C language is given in the Appendix C. The inputs to the program are motor parameters like stator and rotor resistances, inductances, moment of inertia of the coupled drive system, reference flux, reference speed, and reference dc link voltage. The simulation plots are given in next few pages.

Fig 3.9 shows the speed response, the dc link voltage and the electromagnetic torque. In the simulation the reference speed is 500 rpm and reference dc link voltage 120 volts. The dc link voltage and speed decreases at 1s due to the applied load torque. After that, the dc link voltage and the speed recover to their respective reference values. Fig. 3.10 shows the source current and source voltage. The input power factor is found to be unity. At 1s, the magnitude of source current is increased due to the applied load torque. At zero load torque, a small magnitude of current flows due to stator losses in induction motor and due to losses in the converter.

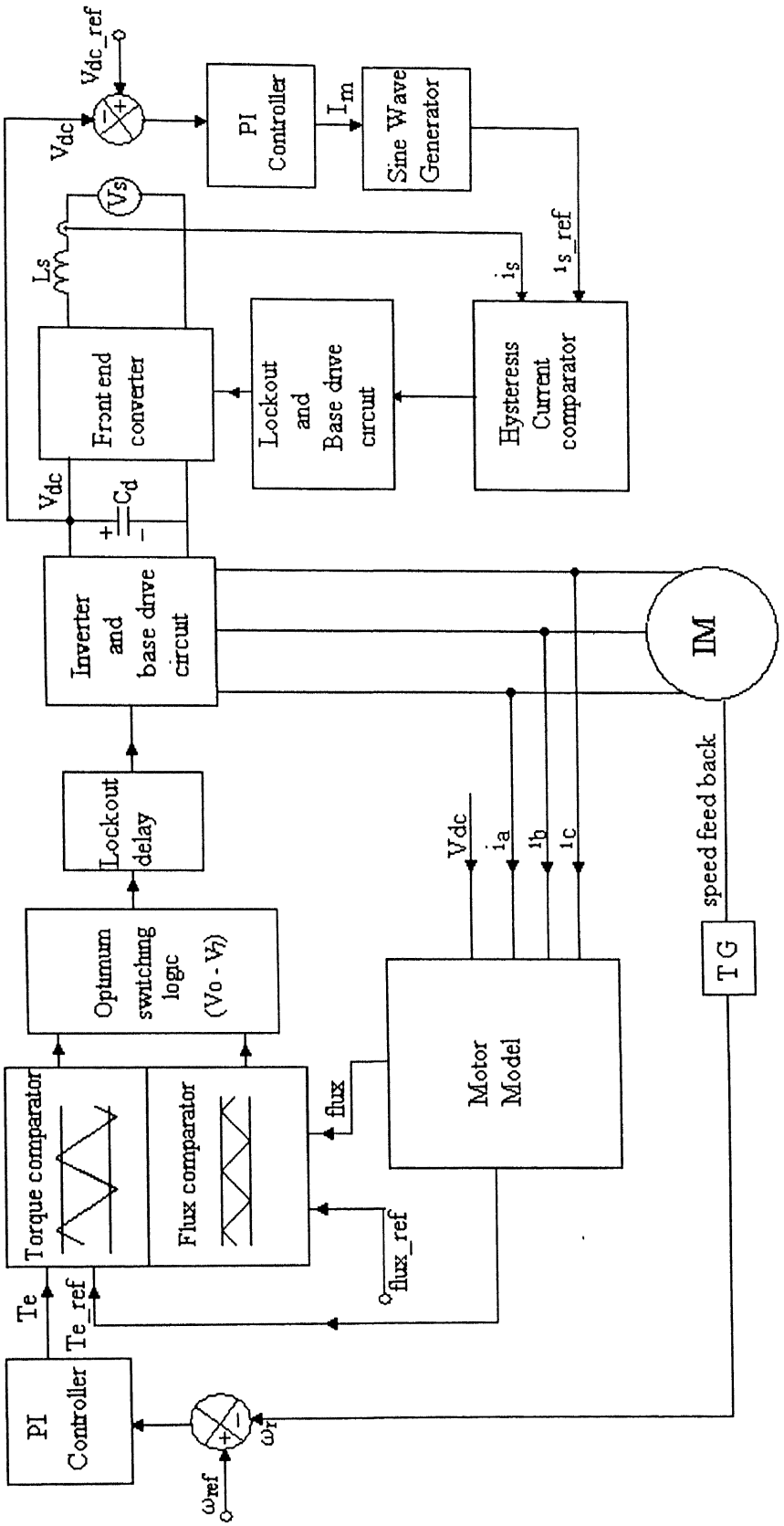

Fig 3.7 Block diagram of the DTFC with SLC as a front end converter

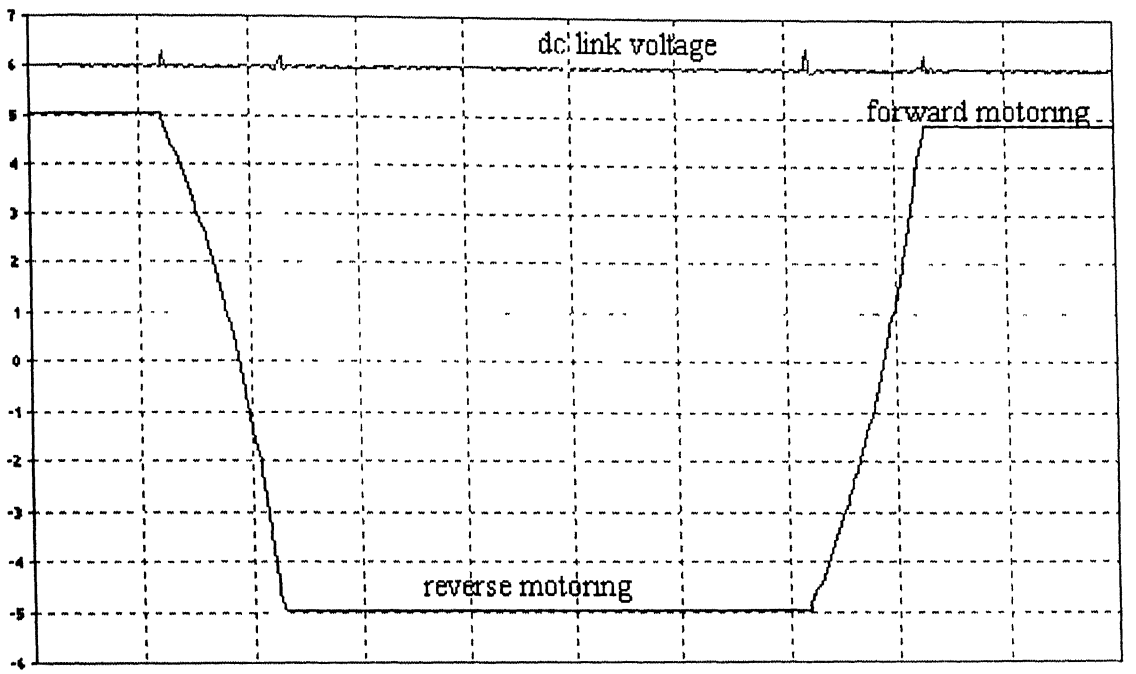

y- axis 1 div = 20 volts (dc link voltage)

1 div = 100 rpm (motor speed)

Fig. 3.18 Forward motoring and reverse motoring

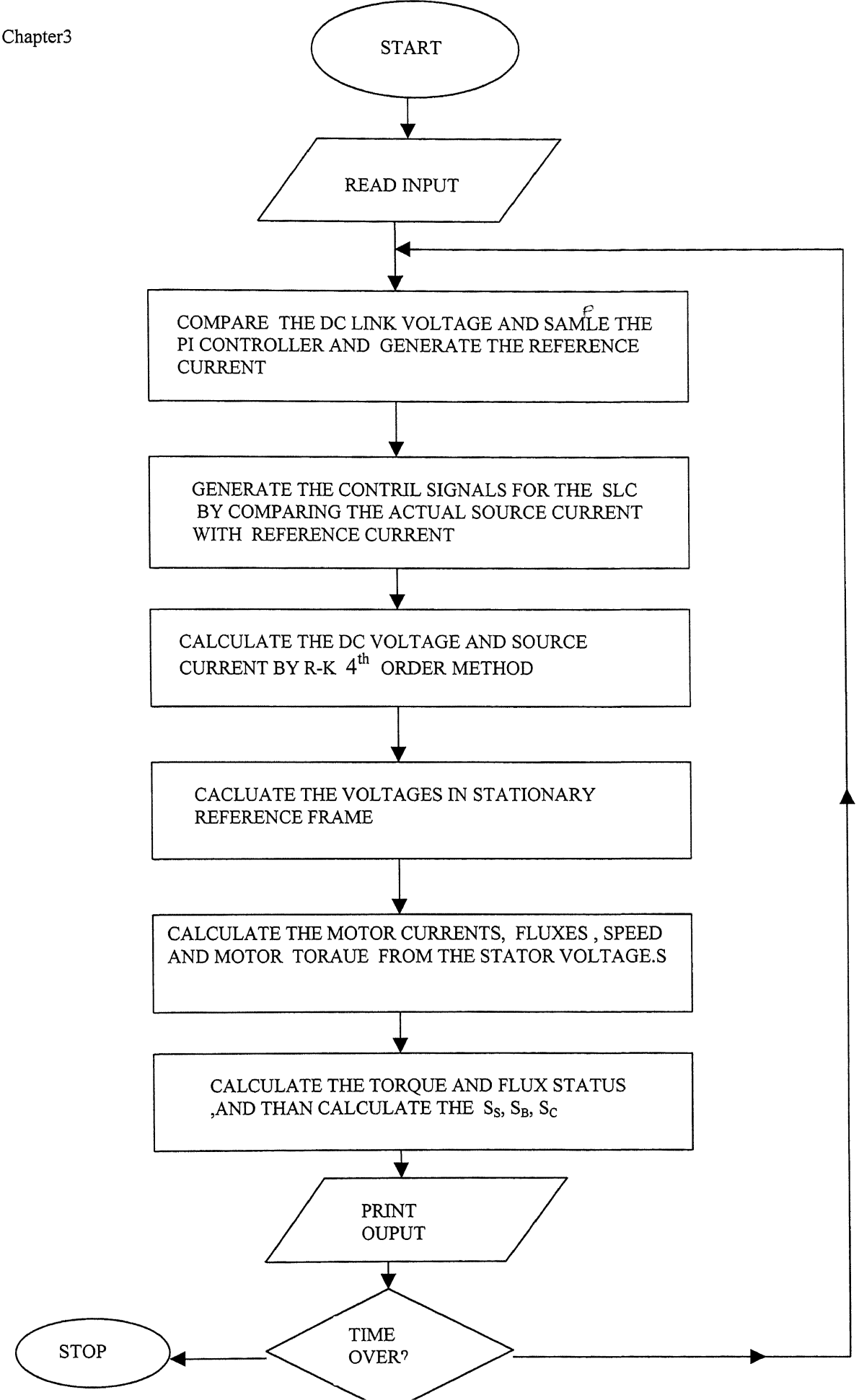
START
READ INPUT
COMPARE THE DC LINK VOLTAGE AND SAMLE THE PI CONTROLLER AND GENERATE THE REFERENCE CURRENT
GENERATE THE CONTRIL SIGNALS FOR THE SLC BY COMPARING THE ACTUAL SOURCE CURRENT WITH REFERENCE CURRENT
CALCULATE THE DC VOLTAGE AND SOURCE CURRENT BY R-K 4th ORDER METHOD
CACLUATE THE VOLTAGES IN STATIONARY REFERENCE FRAME
CALCULATE THE MOTOR CURRENTS, FLUXES , SPEED AND MOTOR TORAUE FROM THE STATOR VOLTAGE.S
CALCULATE THE TORQUE AND FLUX STATUS ,AND THAN CALCULATE THE S_S, S_B, S_C
PRINT OUPUT
TIME OVER?
STOP

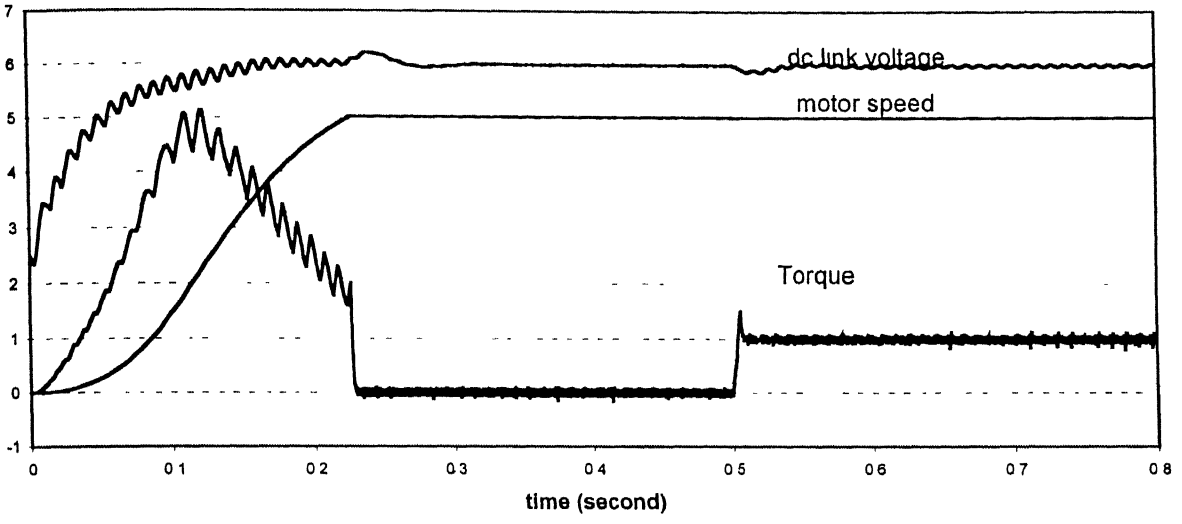

y axis: 1 div = 20 volts (dc link voltage)
1 div = 100 rpm (motor speed)
1 div = 1 Nm (torque)

Fig. 3.9 Dc link voltage and motor speed for change in load torque at 0 5s

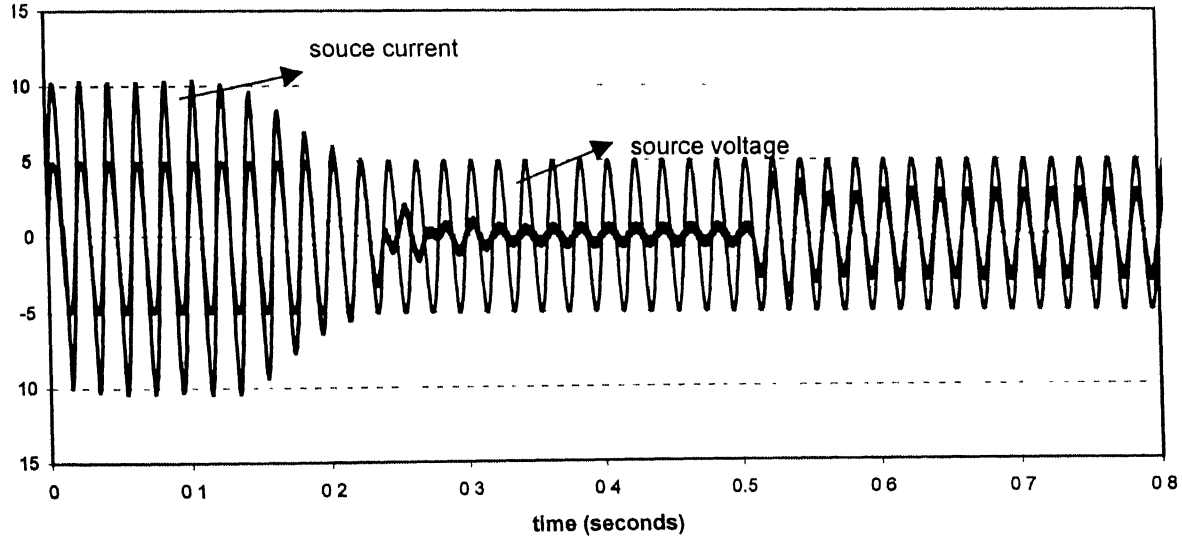

y axis : 1 div = I amp (source current)
1 div = 10 volts (source voltage)

Fig 3 10 Source current source voltage

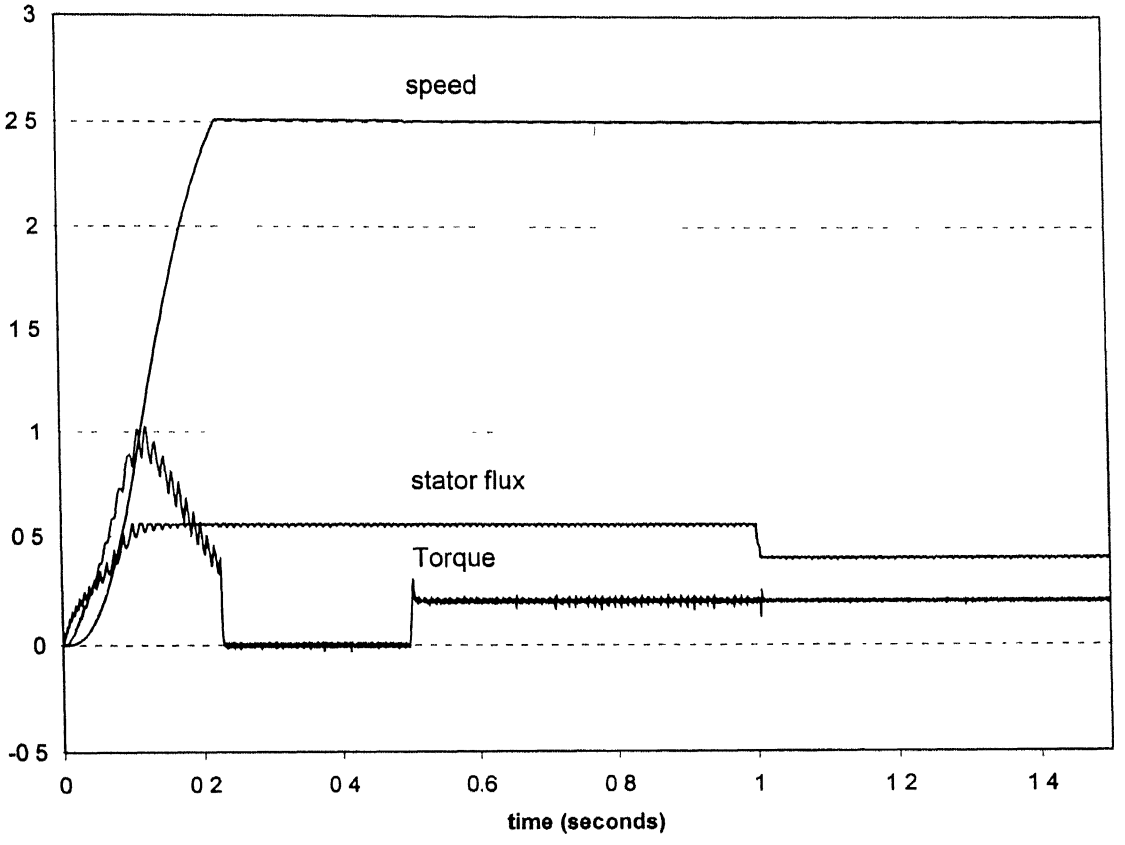

Y axis : 1div = 200 rpm (speed)
1div = 0.5wb (flux)
1div = 5Nm (torque)

Fig . 3.11 Speed response with step change of torque and flux at 500rpm

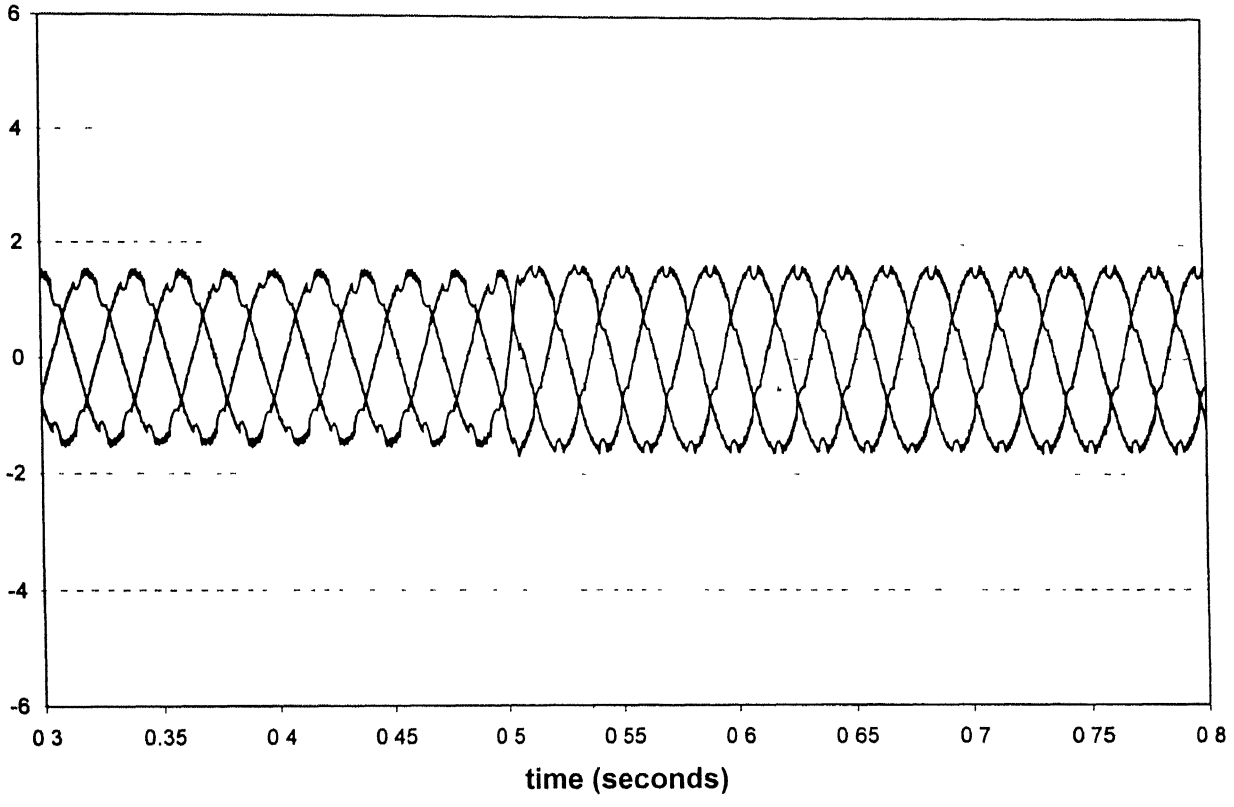

Y axis : 1 div = 2 amp (phase current)

Fig. 3.12 Induction motor phase currents

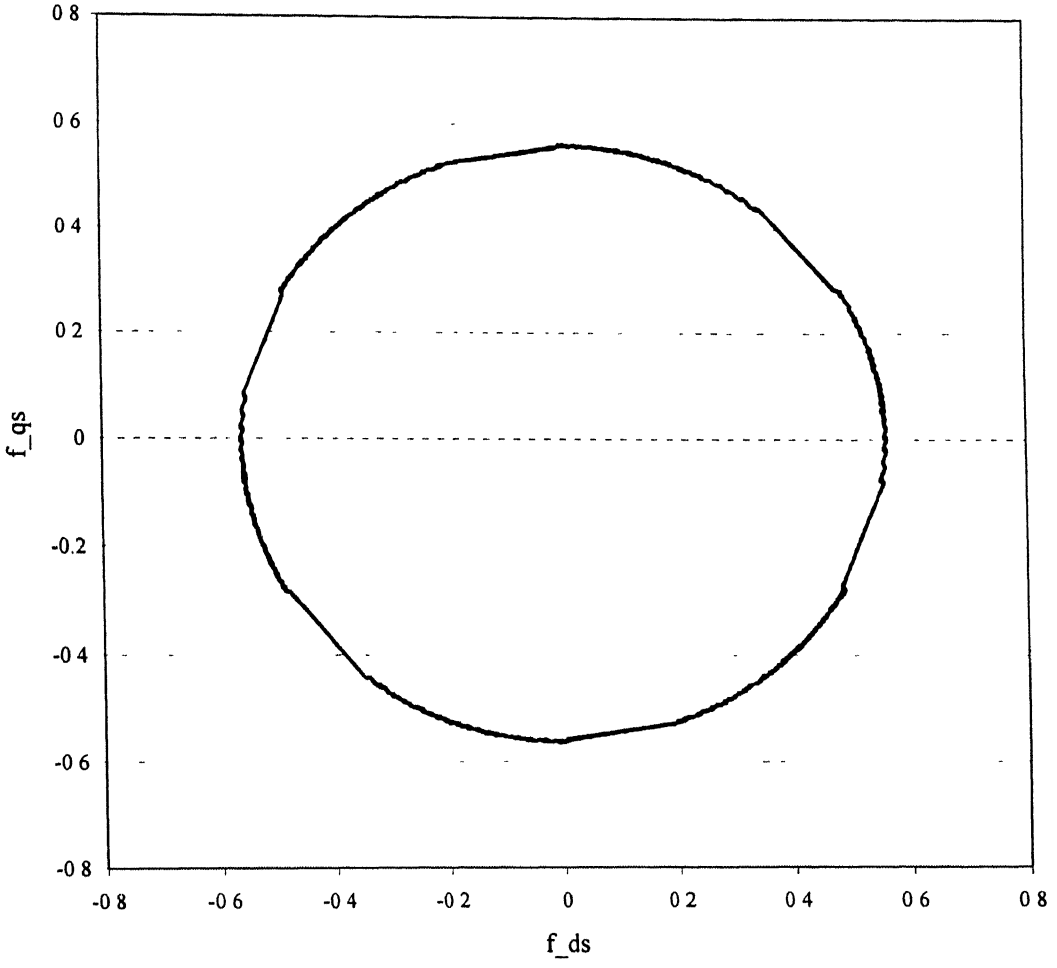

X axis : 1 div = 0.1 wb (d axis stator flux f_ds)

Y axis : 1 div = 0.1 wb (q axis stator flux f_qs)

Fig. 3.13 Stator flux profile during normal operation

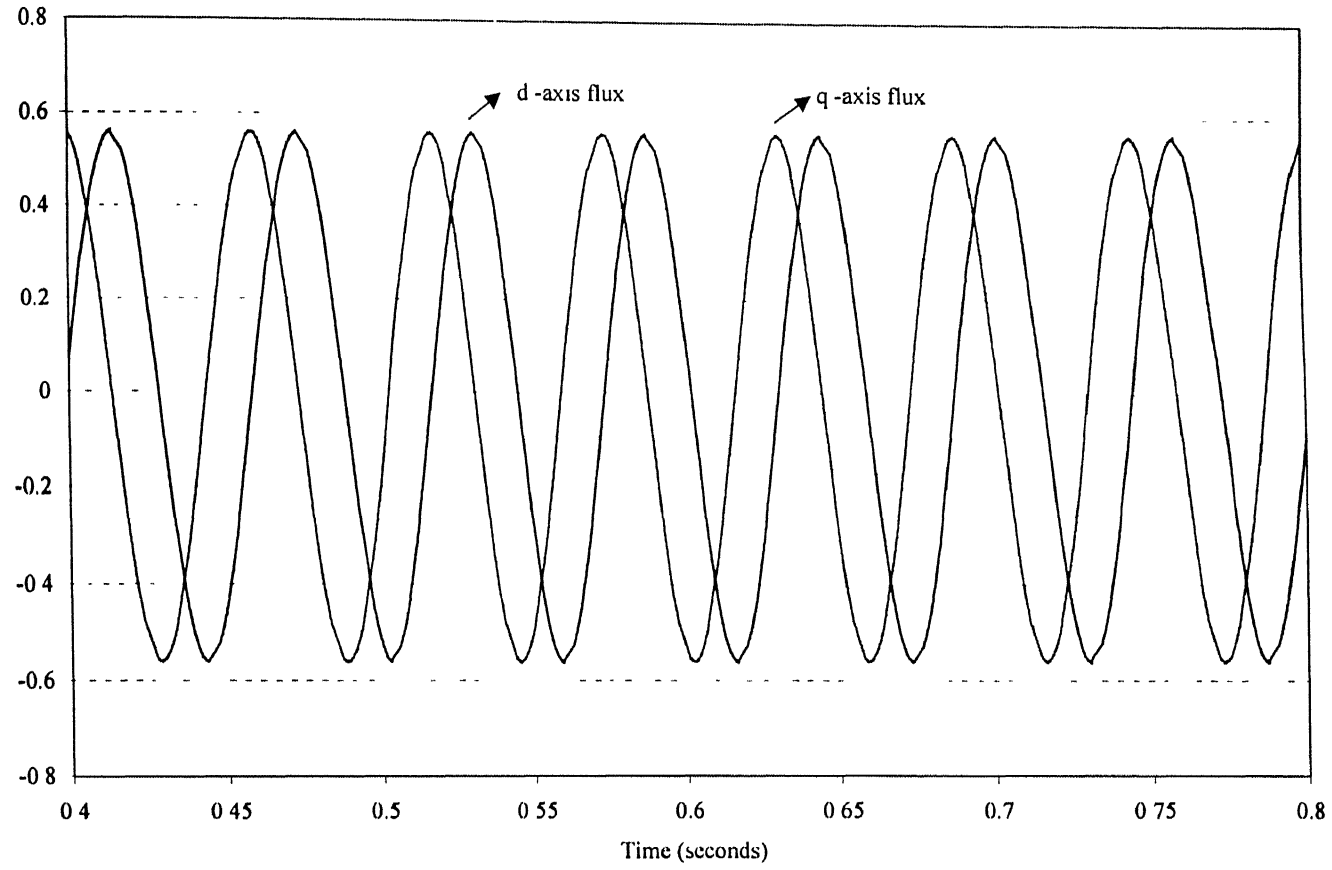

Y axis I div = 0.2 wb (flux)

Fig 3.14 d – axis and q –axis stator fluxes under normal operating condition

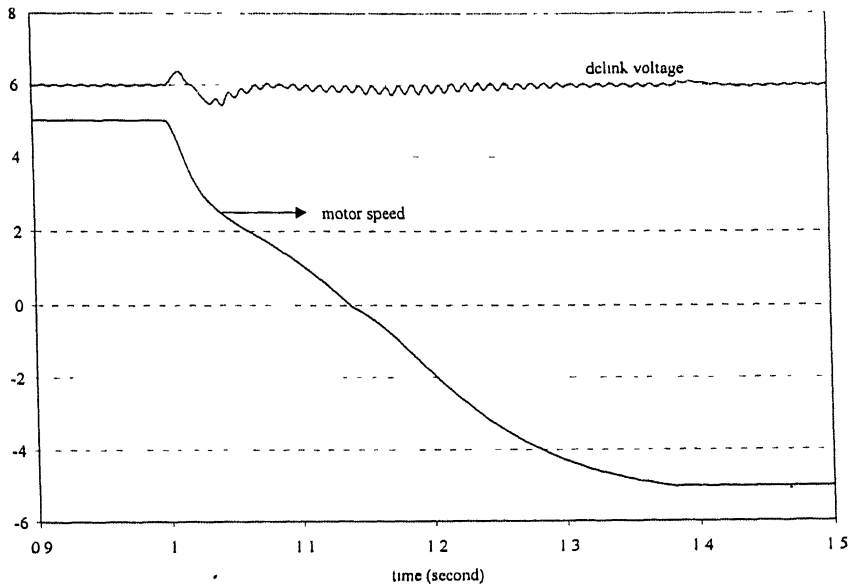

Y axis : 1 div = 20 volts (dc link voltage)

1 div = 100 rpm (motor speed)

Fig. 3.15 Dc link voltage and motor speed during speed reversal (speed reversal at 1s)

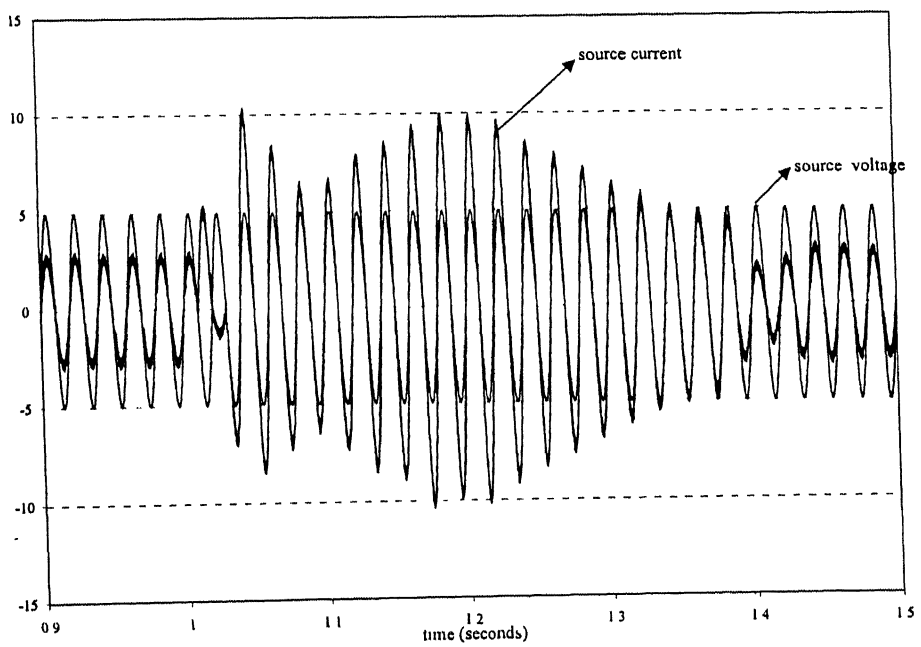

Y axis : 1 div = 1 amp (source current)

1 div = 10 volts (source voltage)

Fig. 3.16 Source current and source voltage during speed reversal (speed reversal at 1s)

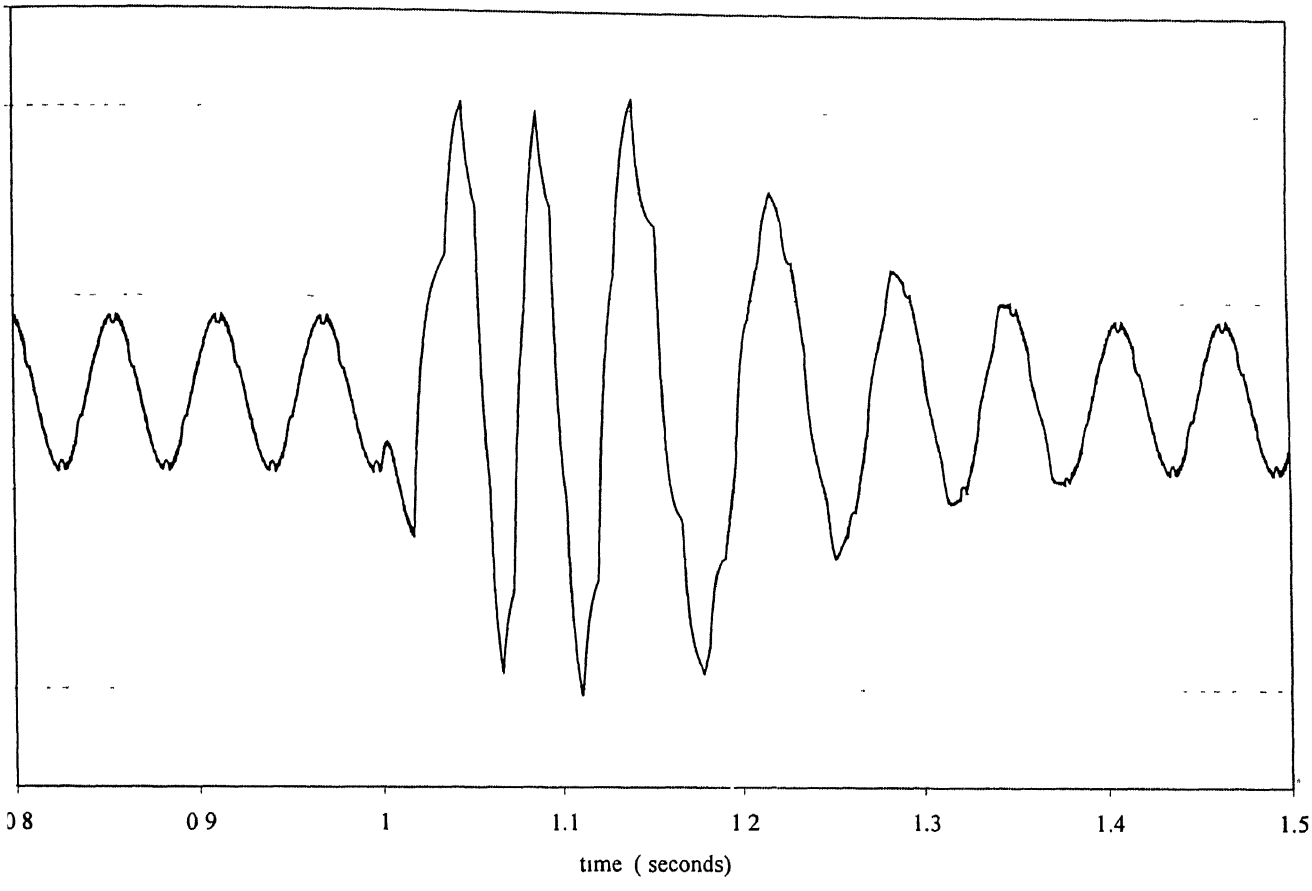

Y axis : 1div = 2 amp (motor phase current)

Fig 3.17 Motor phase current during speed reversal (speed reversal at 1s)

Chapter 4

PC-BASED IMPLEMENTATION OF THE IDUCTION MOTOR DRIVE

4.1 Introduction

In chapter-3 simulation studies have been made for four quadrant DTFC of induction motor drive system. After obtaining the simulation results, it is important to validate the control algorithm under actual working environment. This present chapter gives a detailed description of the experimental setup.

4.2 Power Circuit

The power circuit consists of a 3-phase voltage source inverter (VSI), a single phase single phase synchronous link converter (SLC), and a three–phase squirrel cage induction motor coupled with a dc machine. IGBTs are used to fabricate both the VSI and the SLC. The synchronous link converter (SLC) is fed from the single-phase ac supply through an inductor. A 2200μF capacitor is connected at the dc side of the SLC. Snubber circuits are provided across each IGBT to protect the device from the voltage transients $(\frac{dV}{dt})$. Snubber circuits are realised by a series combination of 24 Ω, and 0.1 μF capacitor connected across each device. A dc tachogenerator is coupled with the induction motor to convert the motor

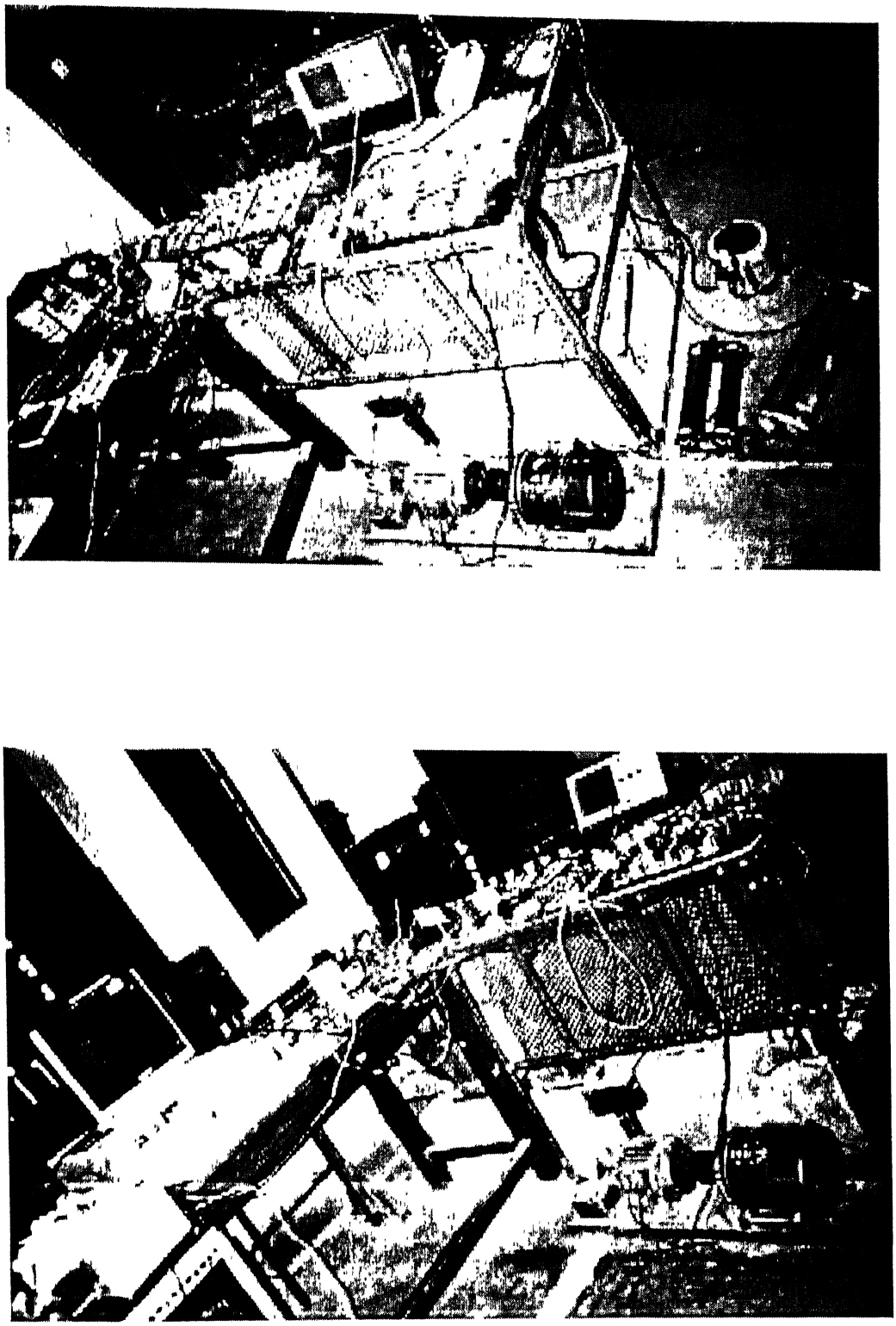

Fig. 4.5 Photographs of the experimental rig

speed into dc voltage. The specifications of the induction motor, dc machine, IGBT, and tachogenerator are given in Appendix –A.

4.3 PC-based Implementation of the Control Circuit

The control circuit mainly consists of an 80486 PC operating at a clock of 100 MHz. The control algorithm is executed in a real time on the PC. The calculations are performed inside the PC. A high-speed data acquisition card ACL – 8112PG has been interfaced with the PC for the of data transfer between PC and the external hardware. In the actual experimental setup, the drive is controlled by a software program. In the PC-based control scheme the data, like motor currents, motor speed, ac source voltage and dc link voltage signals are given to the digital computer through the high speed acquisition card (ACL – 8112PG). The switching status for inverter and the reference source current are generated by calculations are performed inside the computer and are outputted by the output digital and analog ports of the data acquisition card respectively.

4.3.1 ACL - 8112 PG data acquisition card

While using a PC, it is essential to use a certain interfacing card for data transfer . ACL – 8112PG data acquisition card is used in this application. ACL-8112PG is a high performance, high speed multi-function data acquisition card for IBM PC or compatible computers. The ACL – 8112 PG is designed to combine all the data acquisition functions, such as A/D, D/A, D|O, and timer counter in a single board. The high – end specifications of the card makes it ideal for wide range of applications requiring high-speed 12-bit data acquisition at low cost. The features of the ACL-8112PG are given in detail in Appendix–B. This data acquisition card has 16 analog inputs with conversion time of 8μs per channel. Additionally, two analog output channels with external reference, an 8254 timer, 16 digital input/output channels are also present. Following are the primary adjustments made before installing the card in the computer.

1.) Base address setting : - The ACL – 8112PG requires 16 consecutive locations in the I/O address space. Hex 300 - 30F has been selected for the this application.

2.) A/D input range selection: - The card has been configured in single ended analog channel mode with bipolar input having a range of +/ - 5 V.

3.) D/A reference voltage setting: external reference voltage setting.

4.3.2 Sensing of analog signals

The phase currents i.e. i_a, i_b, i_c of the induction motor are sensed by using hall effect sensors (Appendix –A). Hall effect sensors provide isolation between the power circuit and the control circuit. The outputs of the sensor are fed to the A/D channels. Conversion factor for the current sensors is 0.5V/A. A dc tachogenerator is used for speed sensing. The tachogenerator converts speed signal into voltage signal with a conversion factor of 6V/1000 rpm. Since the output of the tachogenerator is not ripple free, a low pass filter is used to filter out the higher order harmonics. The output of the low pass filter is fed to the A/D channel of the card. The dc link voltage is sensed by using a hall effect voltage sensor. The conversion factor of the voltage sensor is 100.

The motor stator flux and torque are calculated inside the PC by using the dc link voltage and the motor currents. The reference source current to the SLC is generated inside the computer by comparing the actual dc voltage and the reference dc link voltage. The reference current is outputted by using D/A channel. The hysteresis current control for the SLC has been implemented outside the PC to optimize the control software. The hardware circuit for the hysteresis band generation and current comparison as shown in Fig 4.1. The output signals of this circuit are used to trigger the IGBTs of the synchronous link converter .

The inverter switching states are evaluated by using the switching logic selection table which has been discussed in chapter 3. The switching signals S_a, S_b, S_c are in digital form. These signals are outputted by using digital output channel of ACL – 8112 PG card. The three signals S_a, S_b, S_c are used to trigger the upper IGBTs of each leg. The complemented signals of S_a, S_b, S_c are used to trigger lower IGBTs of each leg. There should be time delay in two drive signals to the IGBTs of the same leg to avoid momentary

short circuit of the DC bus. A lockout delay circuit, which is shown in Fig. 4.2 has been fabricated. This circuit consists of a dual mono-stable multi-vibrator IC74123, an AND gate IC 7408. The output of the lockout delay is goes to the IGBT driver circuit. The IGBT driver circuit is used to amplify the signals and also to provide the isolation between the control circuit and the power circuit. The base driver circuit is shown in Fig. 4.3, where an opto-coupler is used for the purpose of isolation.

4.4 Block diagram

Fig 4.4 shows the complete block diagram of power circuit and control circuit of PC-based implementation of the four quadrant DTFC of induction motor drive system. As shown in the figure the inputs to the PC are the dc link voltage from the voltage sensor output, ac source voltage for external reference for the D/A channel , and the motor phase currents from the current sensors. The reference source current for the SLC is sent to the hysteresis comparator. The digital outputs for the SLC and VSI are fed to the NOT gates to get the complementary signals. Lockout delay circuits provide a delay of 15 μs between the two signals which are sent to the IGBTs of same leg. The outputs of the lockout delay circuits are given to the respective IGBT base driver circuits to amplify the control signals. The output signals of the base drive circuit are applied to the appropriate bases of the IGBTs of SLC/VSI. The photographs of the experimental rig are shown in Fig. 4.5.

4.5 PC-based Control Program

The PC-based real time control program is given in Appendix C. The program is was written in C language. In the control program, analog signals like motor phase currents, and dc link voltage are inputted. From the sensed signals, the reference current for the SLC, the motor flux status and the torque status are calculated. From the flux and torque status, the switching signals for the inverter are selected from the switching table. The switching signals for the inverter and the reference current for the SLC were sent to the external hardware. One iteration of the control software is executed in 180 μs.

4.6 Conclusions:

Experimental setup for the four quadrant direct torque and flux control of induction motor is explained in this chapter. Data transfer between PC and hardware is achieved by ACL-8112 data acquisition card. The reference current for SLC is generated in side the computer. The hysteresis band generation, and current comparison are made outside the computer. Thus the control software is optimized and has a sampling time of 180μs.

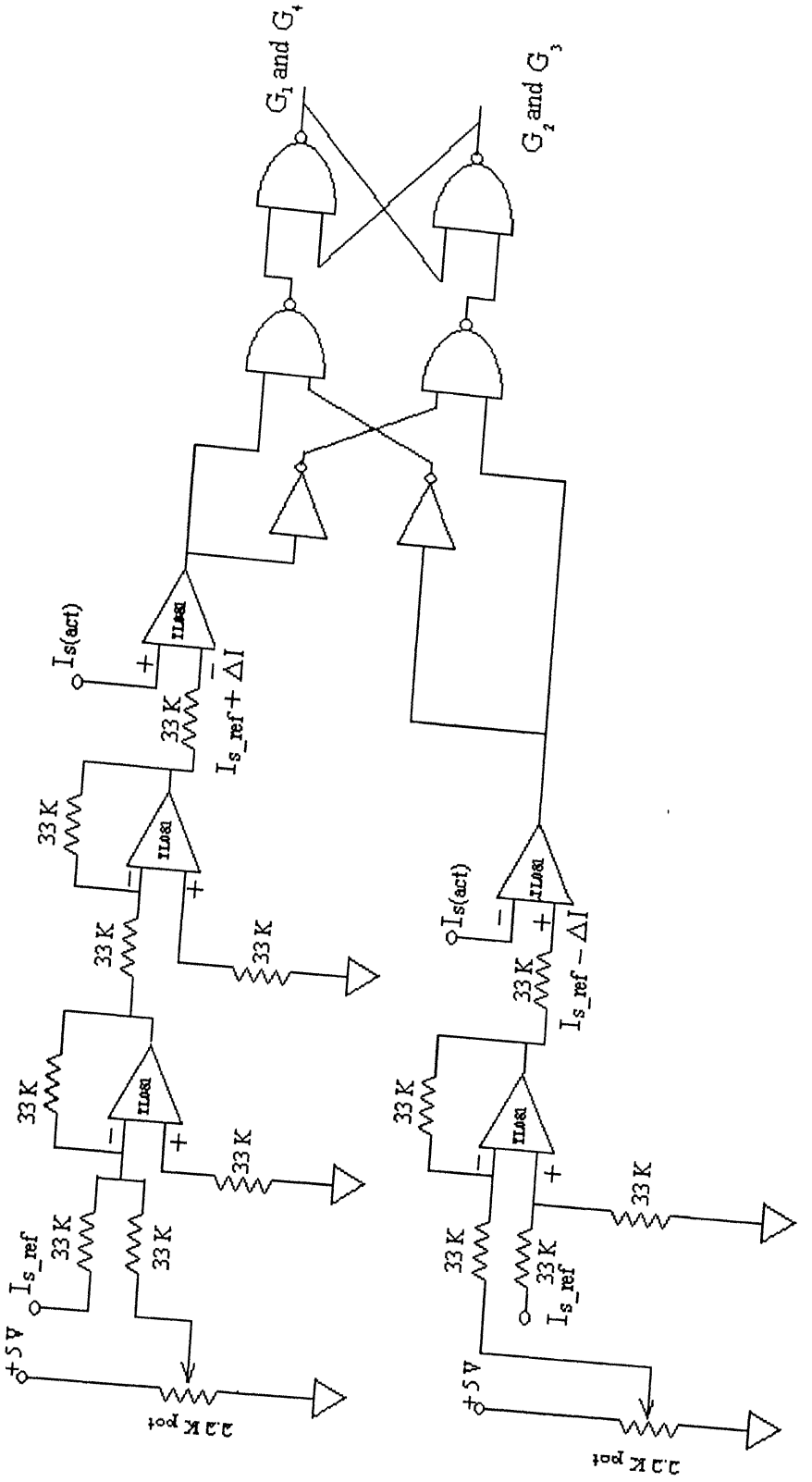

Fig 4.1 Circuit diagram for Hysteresis comparision

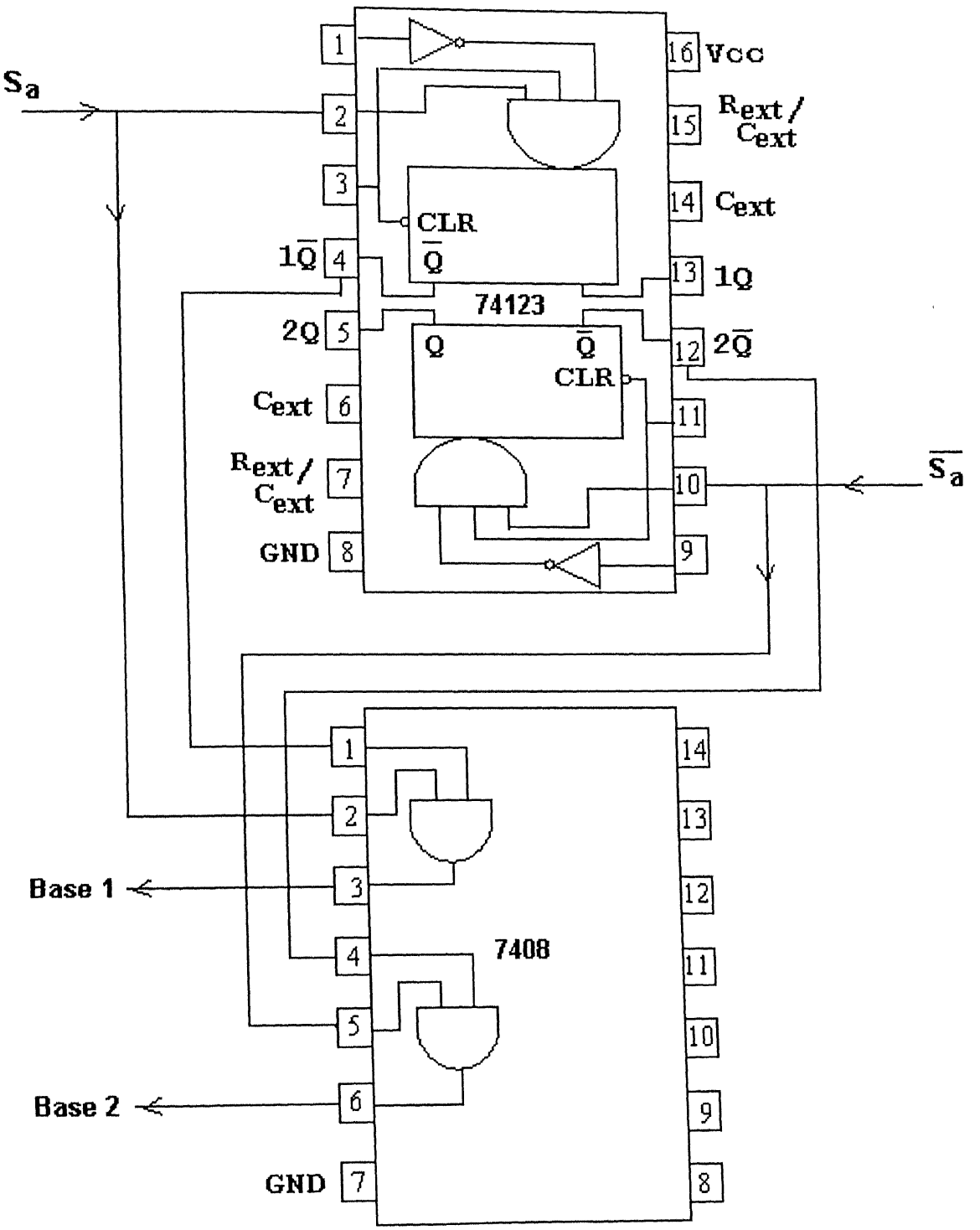

Fig. 4 2 Lockout delay circuit for the phase 'a'

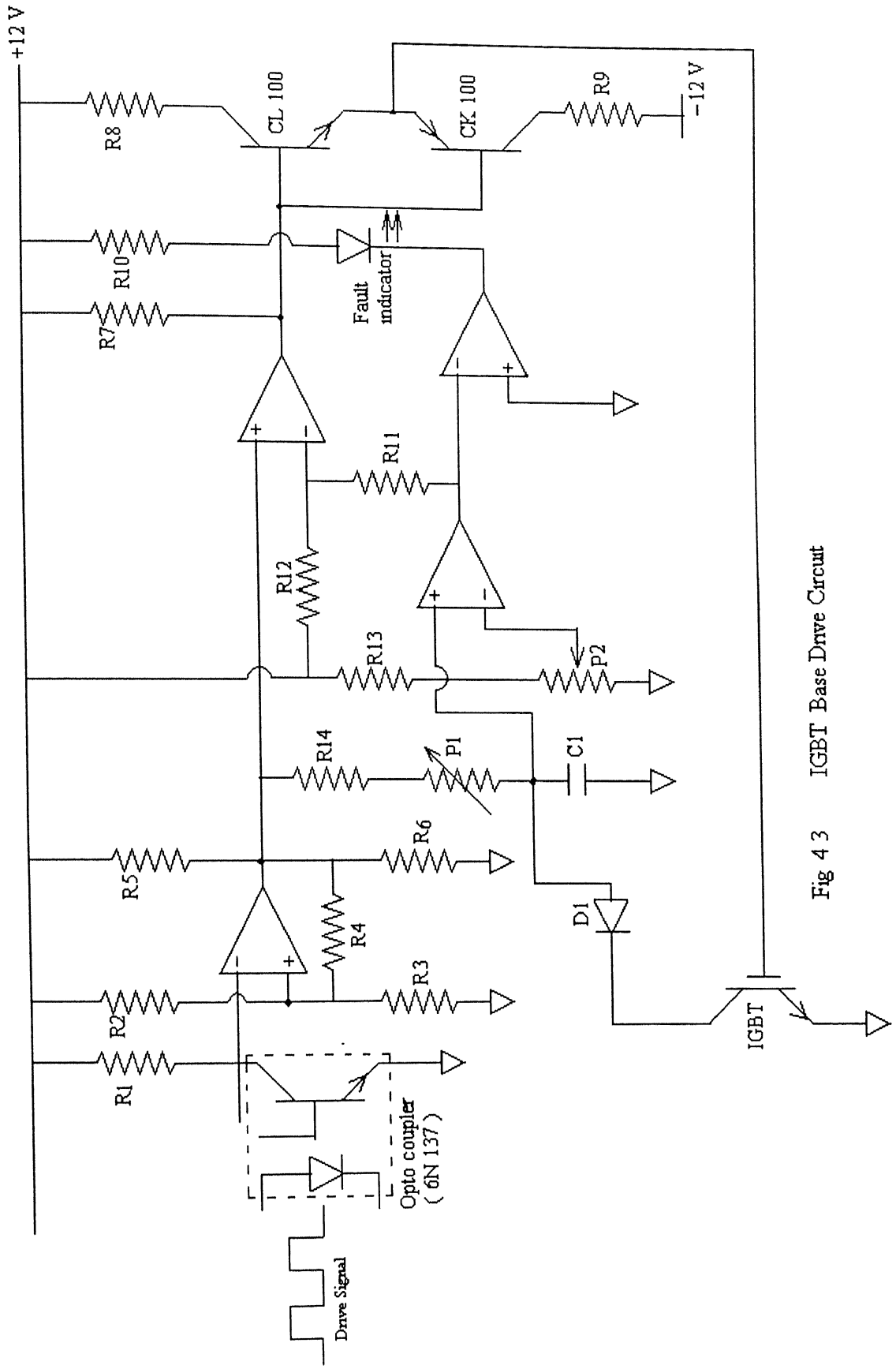

Fig 4 3 IGBT Base Drive Circuit

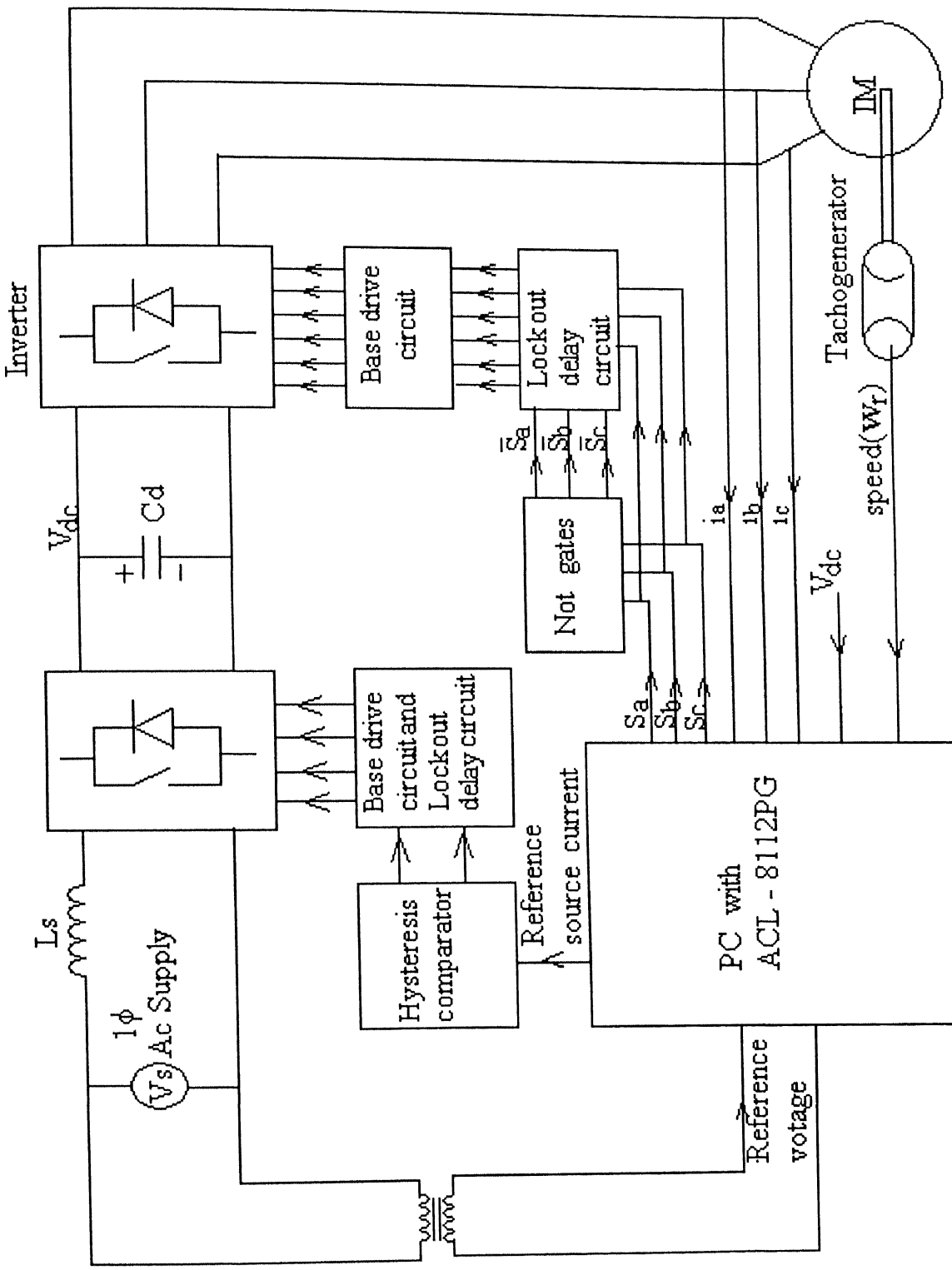

Fig 4.4 Block diagram of power and control circuit of DTFC

Chapter 5

COMPARISON OF SIMULATION AND EXPERIMENTAL RESULTS

5.1 Introduction

The simulated results of the induction motor drive under direct torque and flux control with synchronous link converter as the front end converter show excellent results both for steady state and transient conditions. In the present chapter, typical experimental results are presented and they are compared with the simulation results to validate the design methodology.

The experiment is done on a 3-phase, 415V star connected squirrel cage induction motor which is mechanically coupled with a 230 V, 1500 rpm dc machine for loading purpose. 35V rms voltage is applied to synchronous link converter for ac - dc conversion. Reference dc link voltage is fixed at 100V.

5.2 Under no load conditions:

Fig. 5.1 to Fig. 5.7 are the simulation and experimental results under no load condition. Fig . 5.1 shows that for step change of speed the stator flux is constant and is equal to the reference value of 0.56 wb. Fig 5.2 shows that motor speed is constant for a step change in flux. These results ensure decoupling of torque and flux. Fig. 5.3 shows that the power factor at the source side is unity. Additionally, the source current follows the reference signal which is in phase with the source voltage, within the hysteresis band.

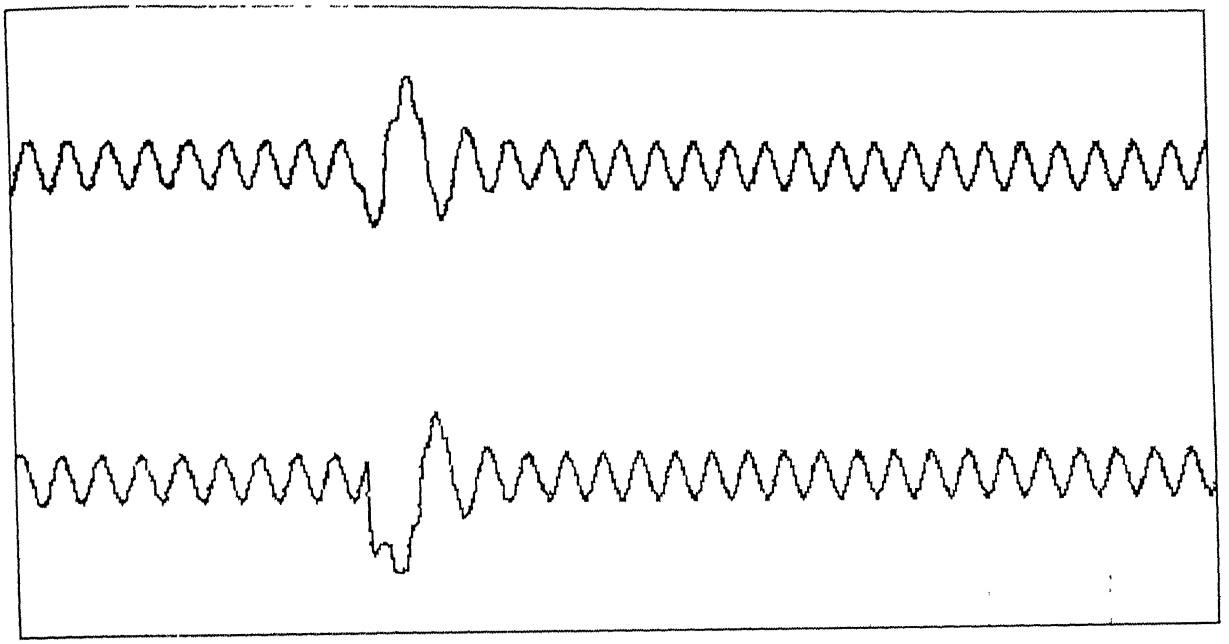

x axis 1 div = 200ms (time)
y axis 1 div = 4 amps (current)

Fig. 5.7a simulated wavefrom

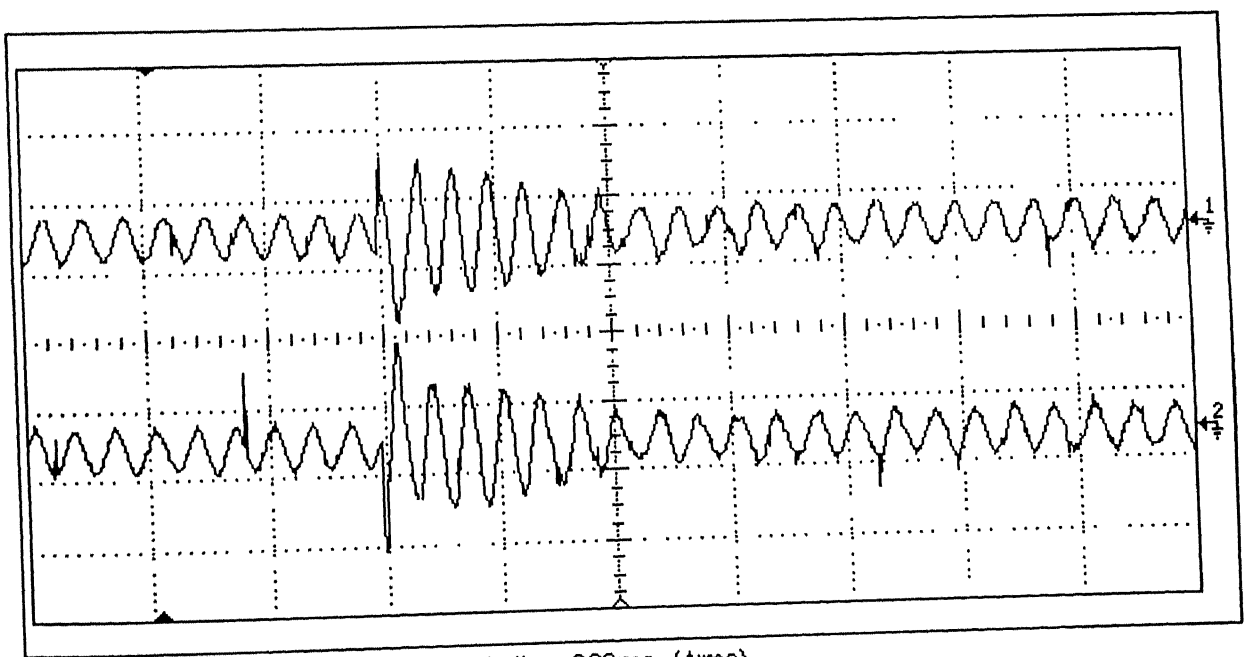

x axis 1 div = 200ms (time)
y axis 1 div = 4 amps (current)

Fig. 5.7b simulated waveform

Fig. 5.7 Motor phase currents during speed reversal

5.4 shows that the motor phase currents are nearly sinusoidal. In DTFC the motor currents are indirectly controlled by controlling the torque directly. Fig. 5.8 shows that the magnitude of flux is constant and flux profile follows the circular path.

Speed reversal

Simulated and experimental waveforms of the speed response, the flux response, the dc link voltage, and motor phase currents for the step change of speed command from +500 rpm to –500 rpm are shown in Fig 5.5, Fig 5.6 and Fig 5.7. The speed change from +500 rpm to –500 rpm takes place within 0.3s. The speed response is found to be fast. The machine is operating in regenerating mode from speed from +500rpm to Zero speed. During this transient period, the motor phase currents are high, as shown in Fig 5.7. The flux is nearly constant during this transient and is equal to the reference value 0.56 wb. This shows the de-coupling of torque and flux and establishes that the operation is similar to that of a separately excited dc machine. During the transient period, the stator losses are more due to high copper-losses in the stator resistance of the induction motor. Four quadrant operation of the drive system is shown in Fig. 5.12.

5.3 Step change in torque command

The load on induction motor is applied by connecting a resistive load to the dc generator, which is coupled to the motor. To bring about a step change in torque command, dc generator coupled to the induction motor was loaded by switching on the field supply while the resistive load is connected to the dc generator. In Fig 5.9, it is shown that as the load is applied on motor, the dc link voltage and speed decreases, soon after they come to their reference values. The settling time depends upon the PI controller gain. In Fig 5.10 and Fig.5.11, the motor phase currents and source current waveforms under the loaded condition, are shown.

5.4 Conclusion

The simulation and experimental results are compared in this chapter and experimental results are matched with simulated results. The important observation is that power factor at source side is unity in the steady state. The speed response of motor is

very fast. From the results, it is seen that the machine is under de-coupled control where the torque and flux can be controlled independently.

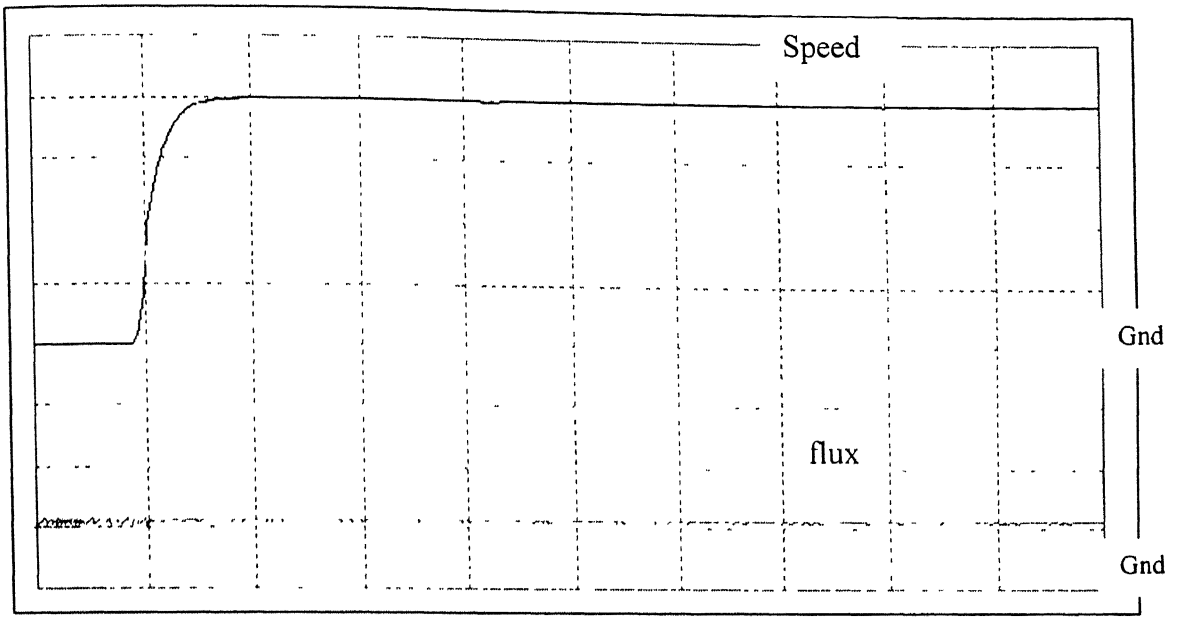

x- axis 1 div = 1s (time)
y- axis 1 div = 125 rpm (motor speed)
1 div = 0.5 wb (motor flux)

Fig. 5.1a Simulated waveform

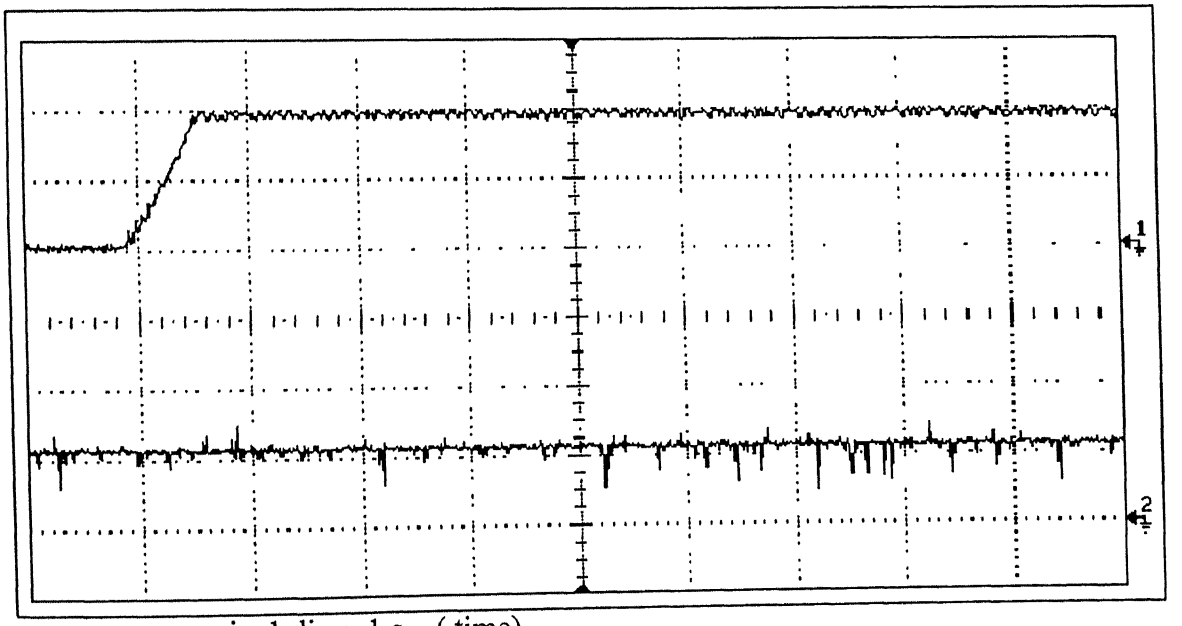

x -axis 1 div = 1 s (time)
y-axis 1 div = 250 rpm. (motor speed - Channel 1)
1 div = 0.5 wb. (stator flux - Channel 2)

Fig. 5.1b Experimental waveform

Fig. 5.1 Flux response during step change of speed from 0 rpm to 500rpm

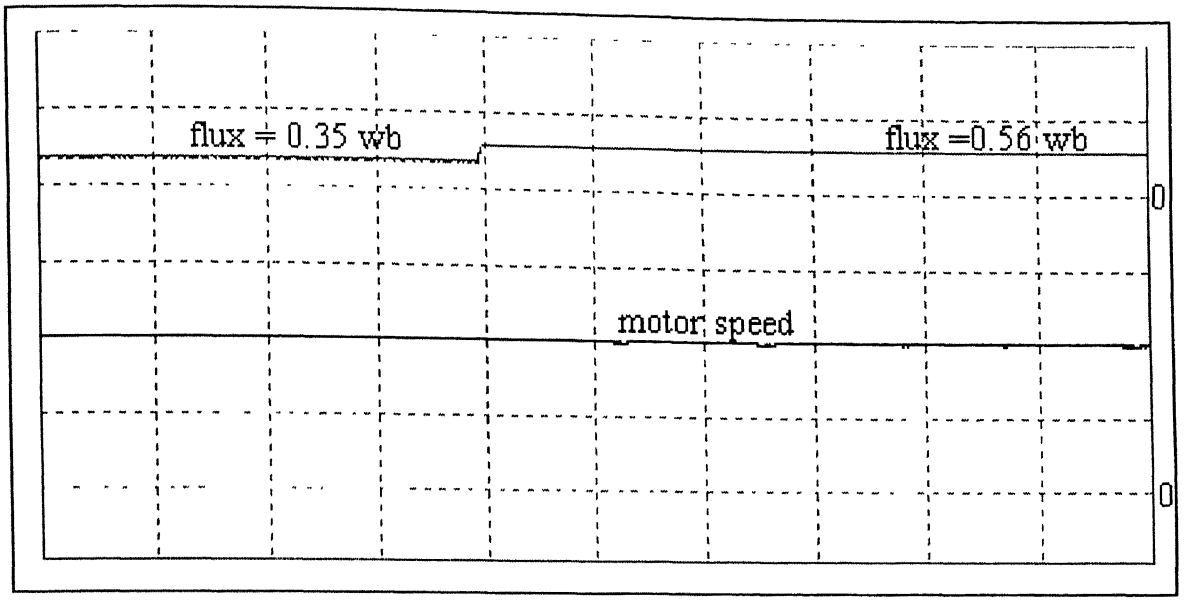

x -axis 1 div = 2 s (time)
y-axis 1 div = 1.0 wb (stator flux)
1 div = 250 rpm (motor speed)
Fig. 5.2a Simulated waveform

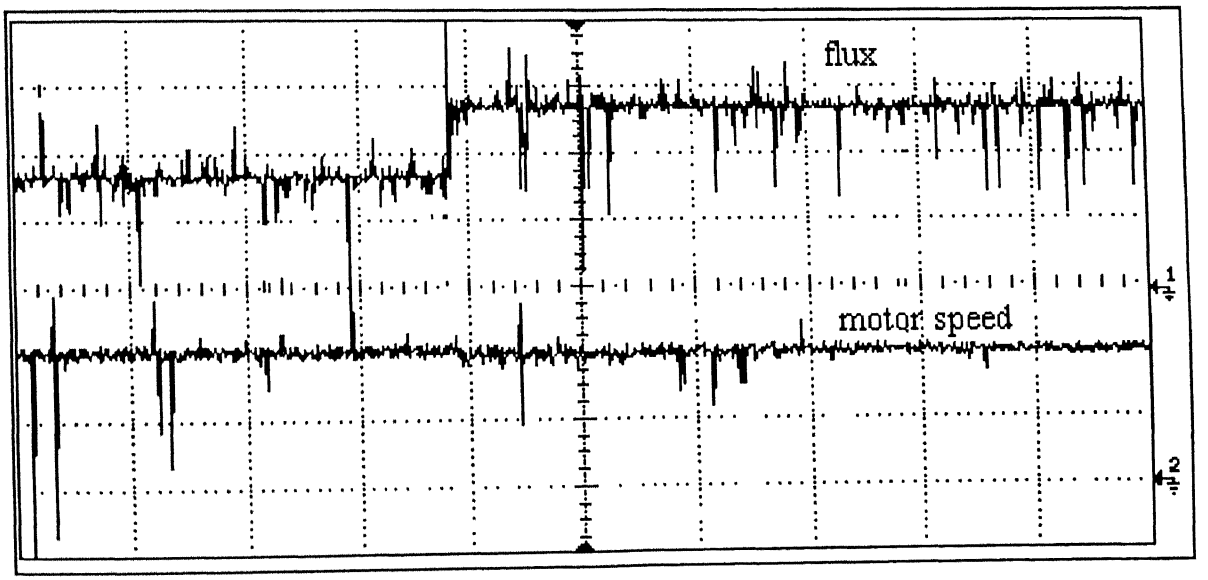

x- axis 1div = 2s (time)
y- axis 1div = 0.2 wb (stator flux)
1 div = 250 rpm (motor speed)
Fig. 5.2b Experimental waveform

Fig. 5.2 Speed response for step change of flux from 0.35 wb to 0.56 wb

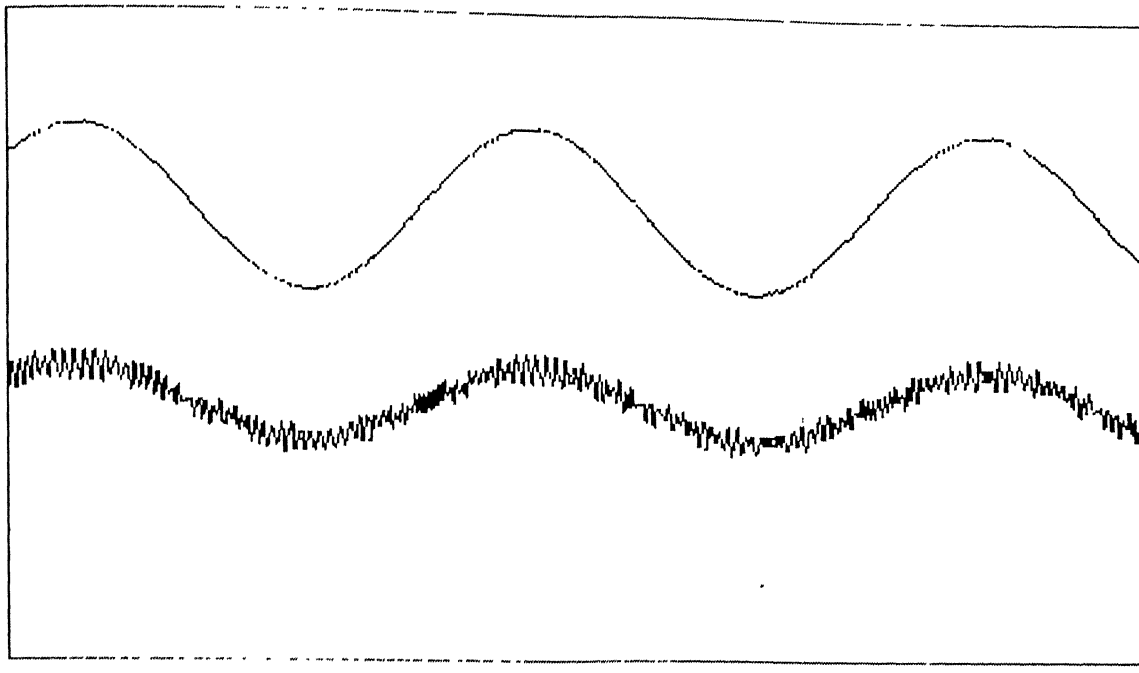

x - axis 1 div = 5 ms (time)
y - axis 1 div = 2 amps (source current)
1 div = 40 volts (source voltage)

Fig. 5.3a Simulated waveform

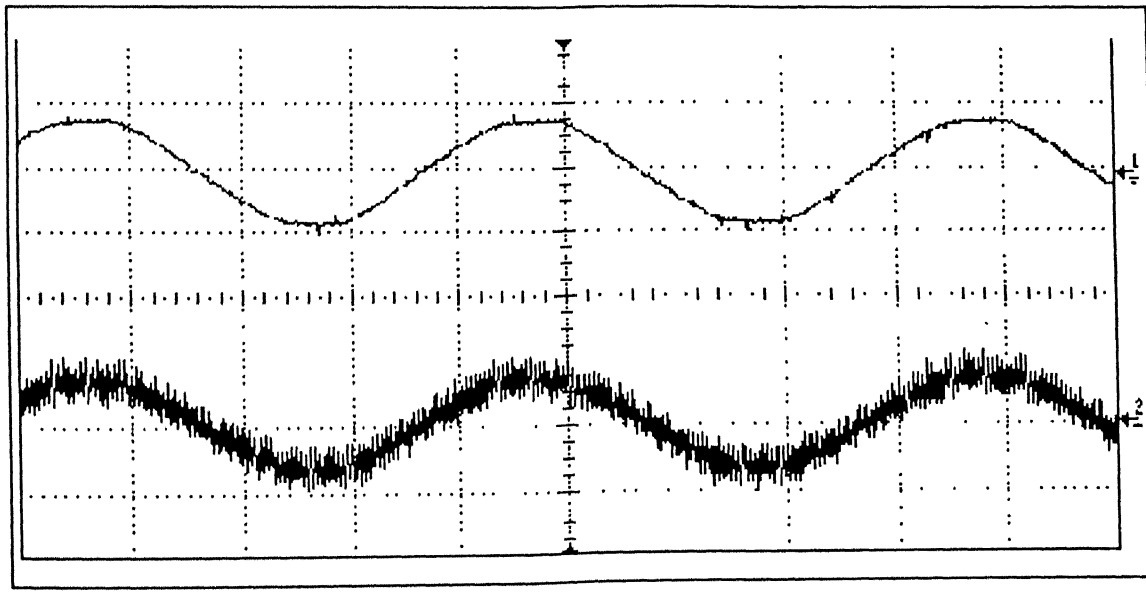

x axis 1 div = 5ms (time)
y axis 1 div = 2 amps (source current -channel 2)
1 div = 10 volts (reference source voltage - channel 1)

Fig. 5.3b Experimental waveform

Fig. 5.3 Source voltage and source current under normal operating condition

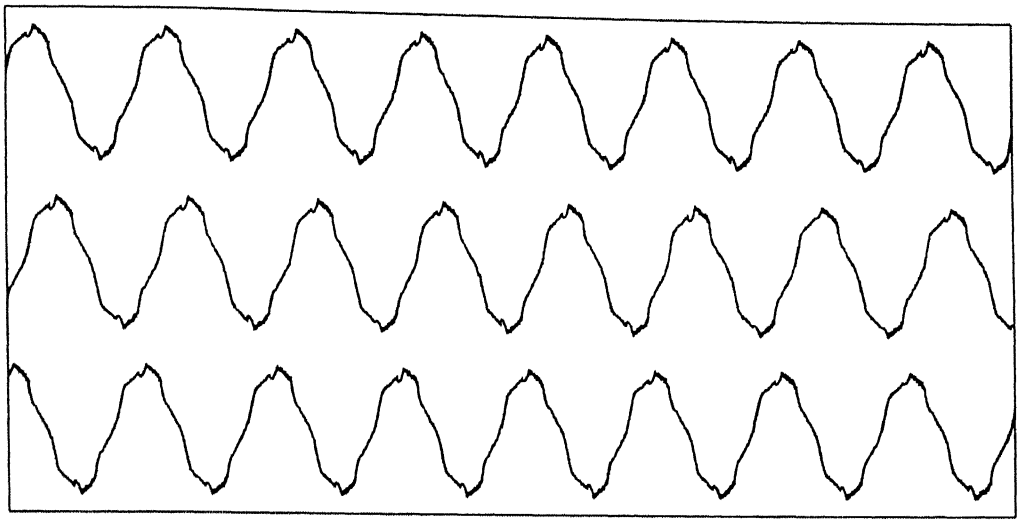

x axis 1 div = 50ms (time)
y axis 1 div = 1 amp(motor currents)

Fig 5 4a simulated waveforms

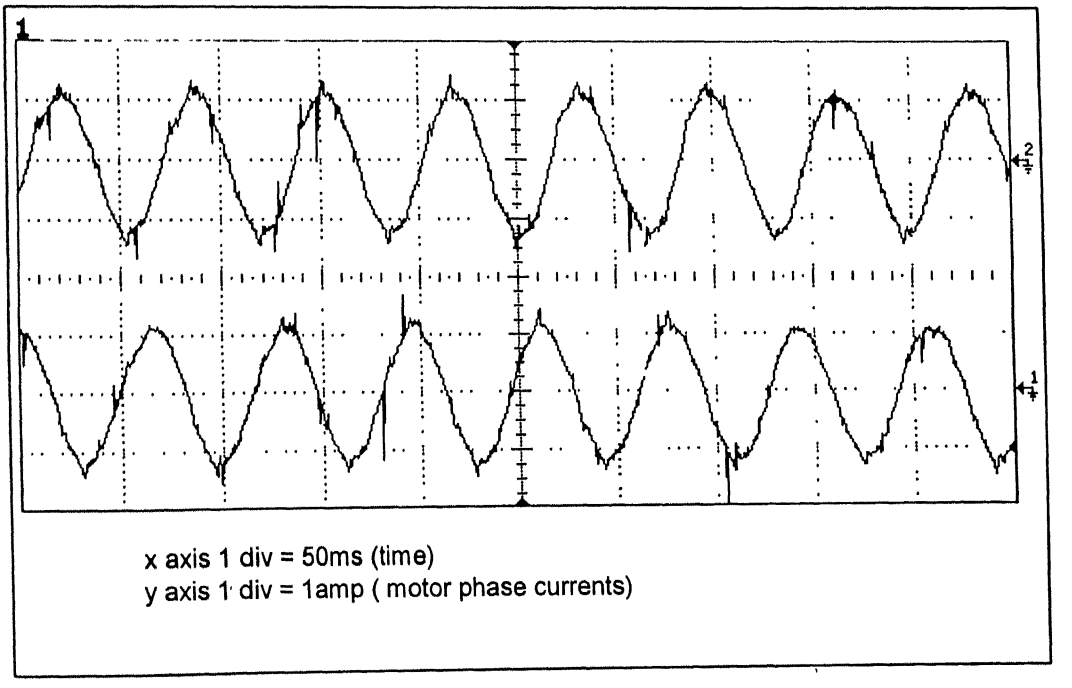

Fig 5 4b experimental waveforms

Fig 5.4 motor phase currents under normal conditions

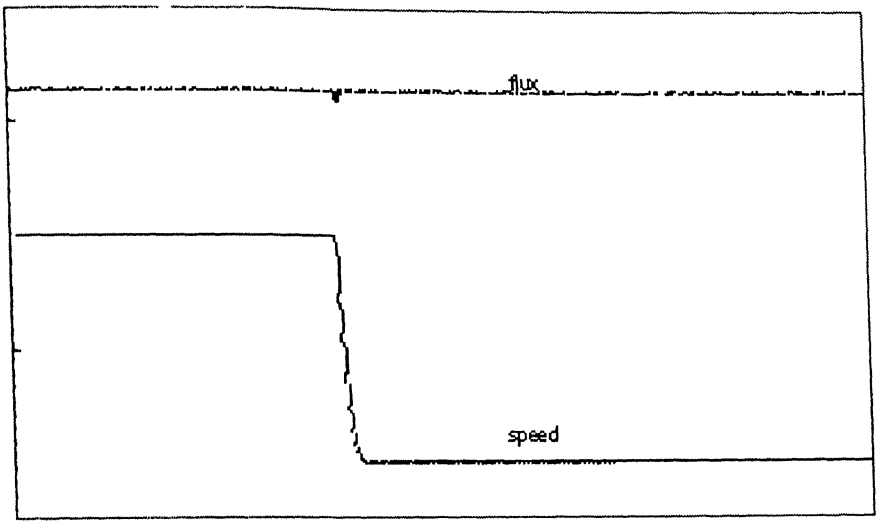

x axis 1 div = 2s (time)
y axis 1 div = 1 weber (flux)
y axis 1 div = 250 rpm (speed)

Fig : 5.5a simulated waveform

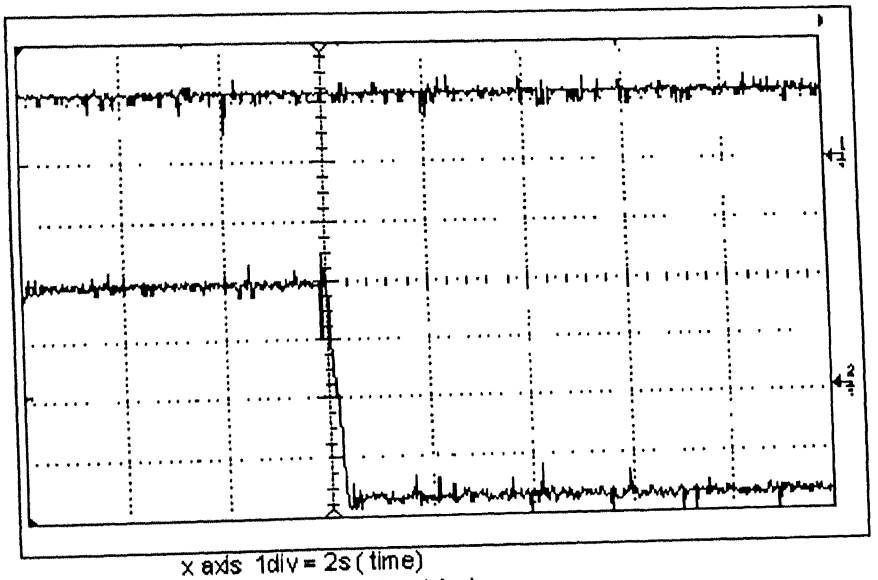

x axis 1div = 2s (time)
y axis 1div = .5 weber (flux)
y axis 1div = 250 rpm (speed)

Fig. 5.5b : experimental waveform

Fig.5 5: flux and speed response durng speed reversal

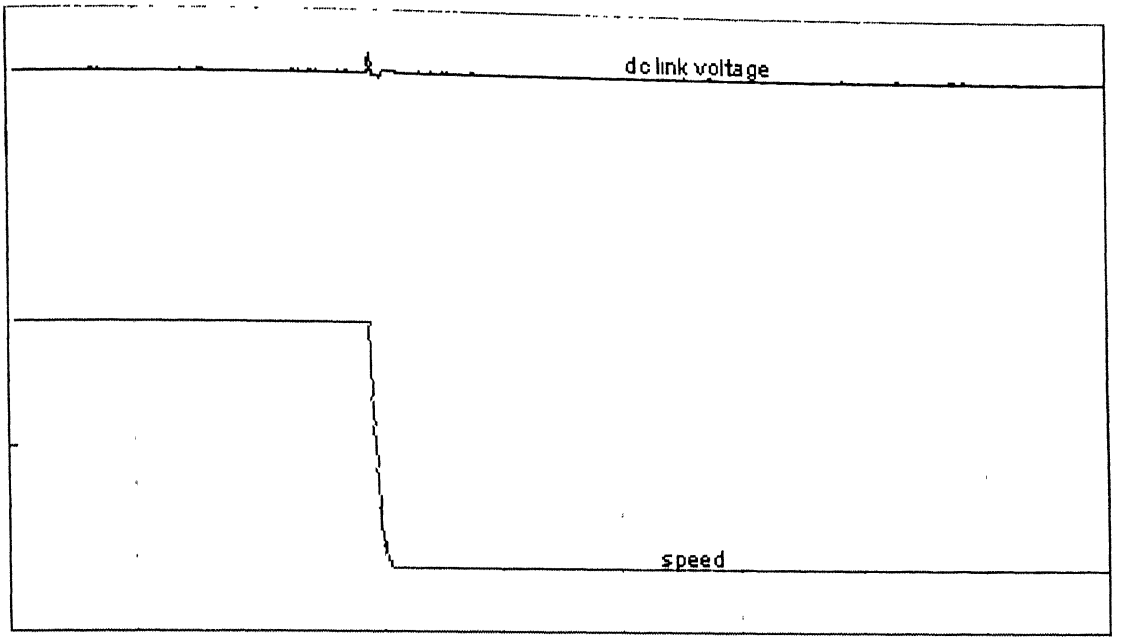

x axis 1div = 2s (time)
y axis 1div = 50 volts (dc link voltage)
y axis 1div = 250 rpm (speed)

Fig. 5 6a simulated waveform

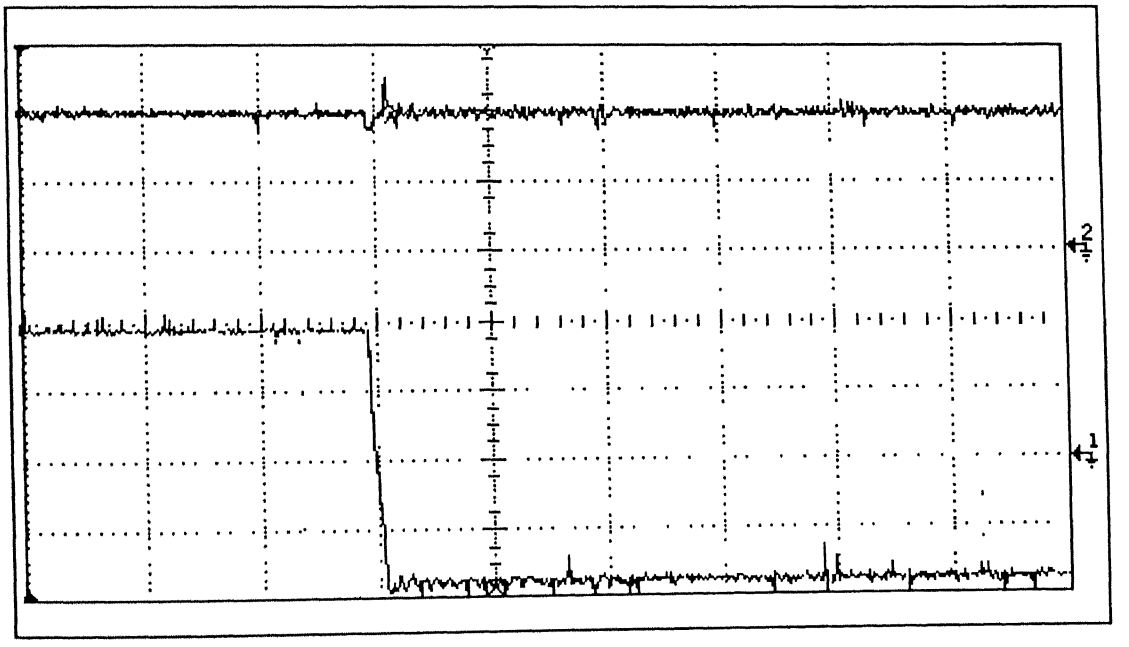

x axis 1 div = 2s (time)
y axis 1 div = 250 rpm (speed channel 1)
y axis 1 div = 50 volts (dc link voltage channel 2)

Fig . 5.6b experimental waveform

Fig. 5.6 Speed and dc link voltage during speed reversal

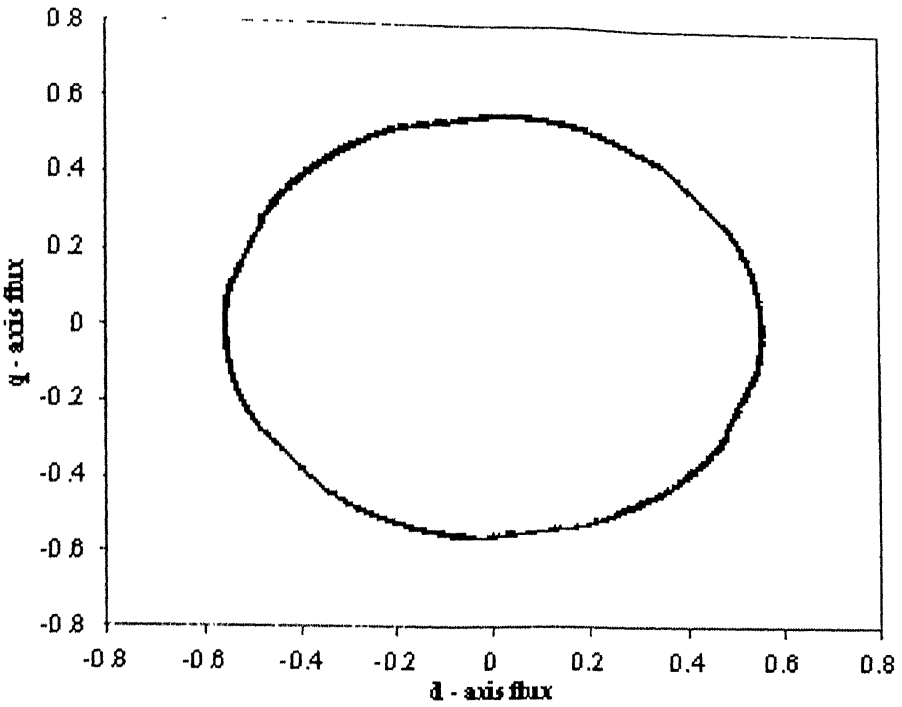

x - axis 1 div = 0.2 weber (d - axis flux)
y - axis 1 div = 0.2 weber (q - axis flux)

Fig. 5.8a Simulation waveform

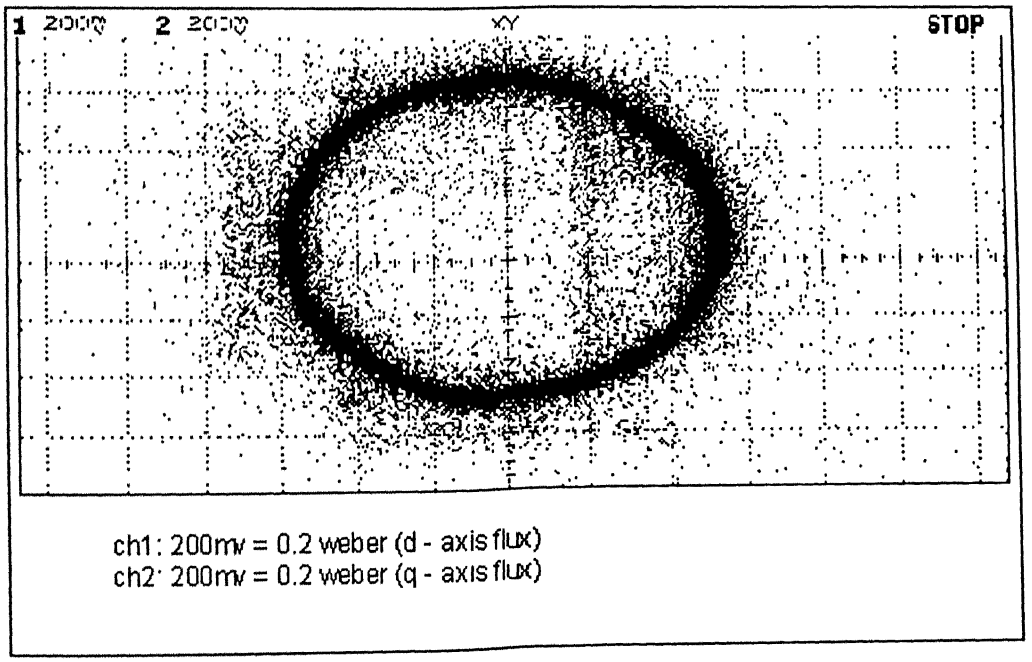

Fig. 5.8b Experimental waveform

Fig. 5.8 d - axis flux verses q - axis flux

[11] A. B. Plunket, "Direct flux and torque regulation in a PWM inverter–fed induction motor drive ," *IEEE Trans. Ind. Appl.*, vol. IA-13, No. 2, pp. 139-146, March / April 1977.

[12] M.P. Kazmierkowski, and A. B. Kasprowicz, "Improved Direct torque and flux vector control of PWM inverter-fed induction motor drives," *IEEE Trans Ind. Electronics,* vol. 42, pp. 344–349, Aug. 1995.

[13] V. T. Ranganathan, "Space vector pulsewidth modulation - A status review," *sadhana,* vol. 22, part 6, pp. 675 - 687, Dec 1997.

[14] I. Takahashi, and T. Noguchi, "A new quick –response and high efficiency control strategy of an induction motor," *IEEE Trans on Ind. Appl.*, vol. IA-22, No. 5, pp. 820 – 827, Sept/Oct. 1986.

[15] A. N. Thakur, S. P. Das, N. K. De, A. K. Chattopadhyay, "Hybrid implementation of indirest vector controlled induction motor and comparison with slip regulated v/f control," i*n proc. NSC , IIT Kanpur 1993.*

[16] Frederickv L, "*Synchronous link Converter and its Applications to Electric Traction*" *M.Tech. Thesis IIT Kanpur, 1998.*

[17] A. Tripathi "*Design, simulation and pc-based implementaton of a direct torque and flux controlled induction motor drive system,*" *M Tech., Thesis IIT Kanpur, 1999*

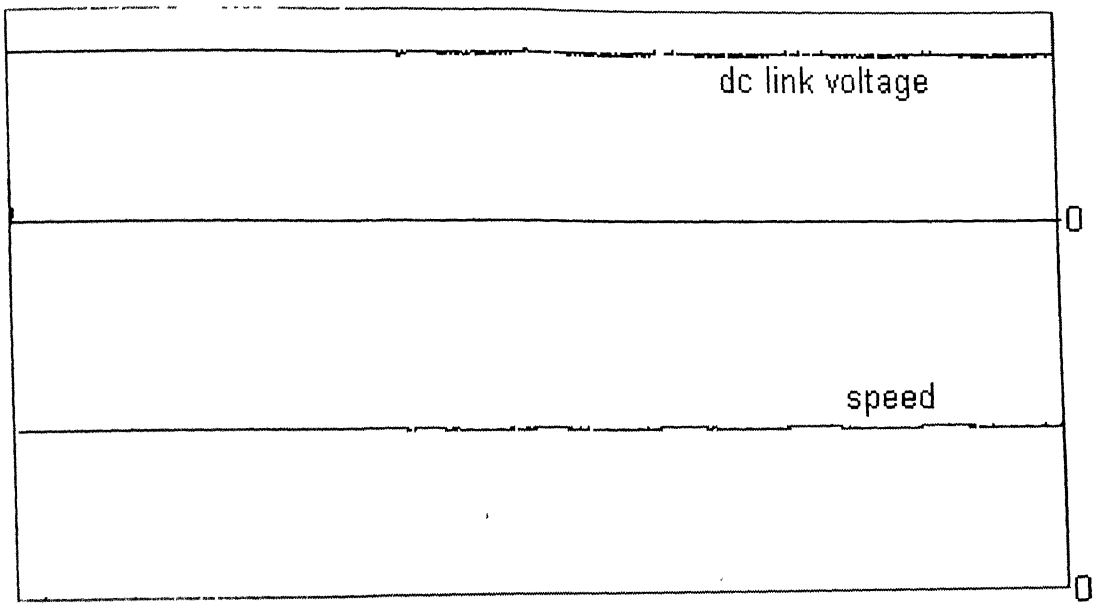

time in seconds

y axis 1 div = 50 volts (dc link voltage)
1 div = 250 rpm (speed)

Fig 5.9a simulated waveforms

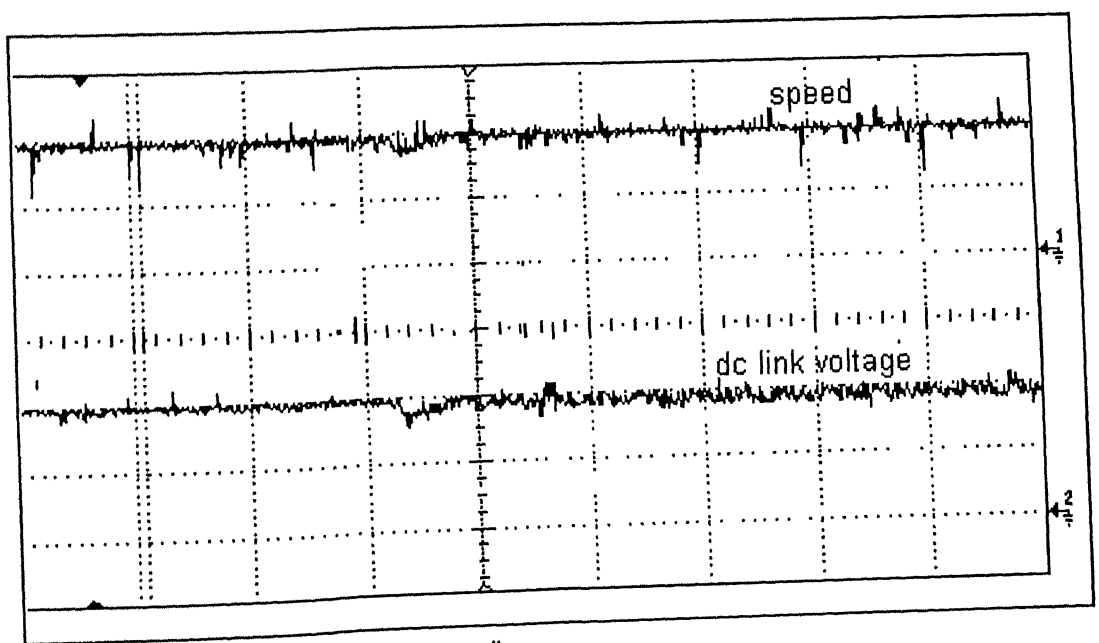

ch1 : 1 div = 250 rpm (speed)
ch2 : 1 div = 50 volts (dc link voltage)

Fig 5.9b experimental waveform

Fig 5.9 speed and dc link voltage response for step change of load

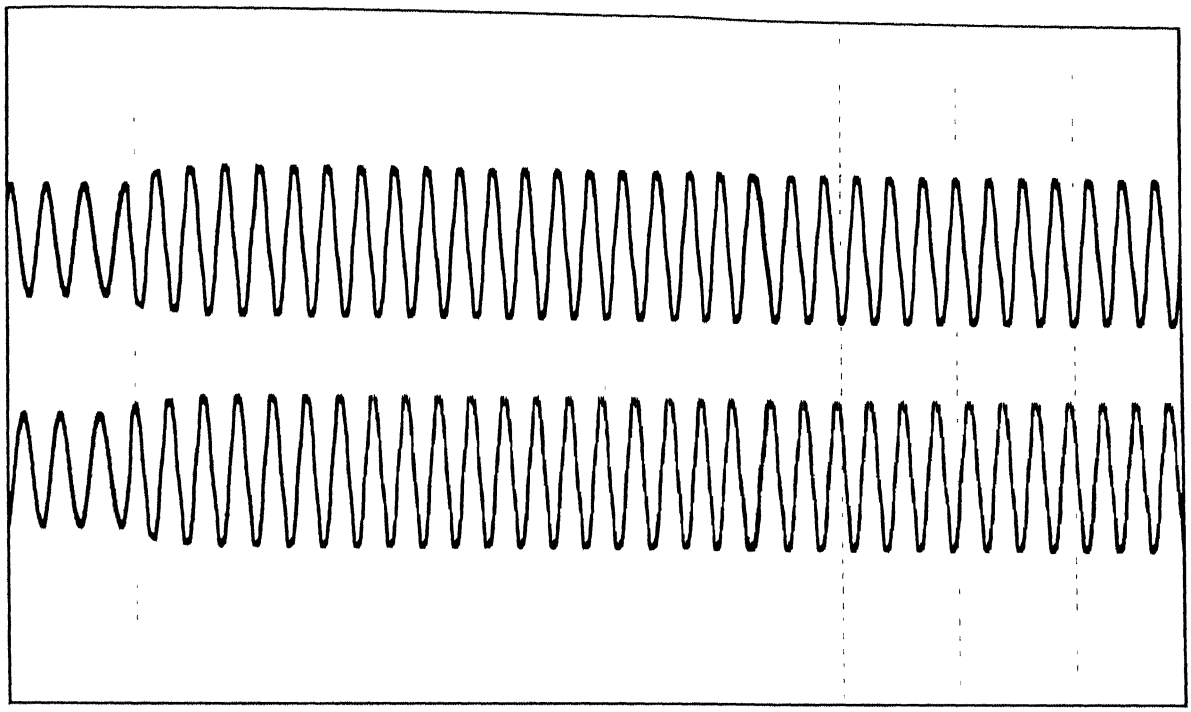

x axis 1 div = 200ms (time)
y axis 1 div = 2amps (motor phase current)
Fig. 5.10a simulated waveform

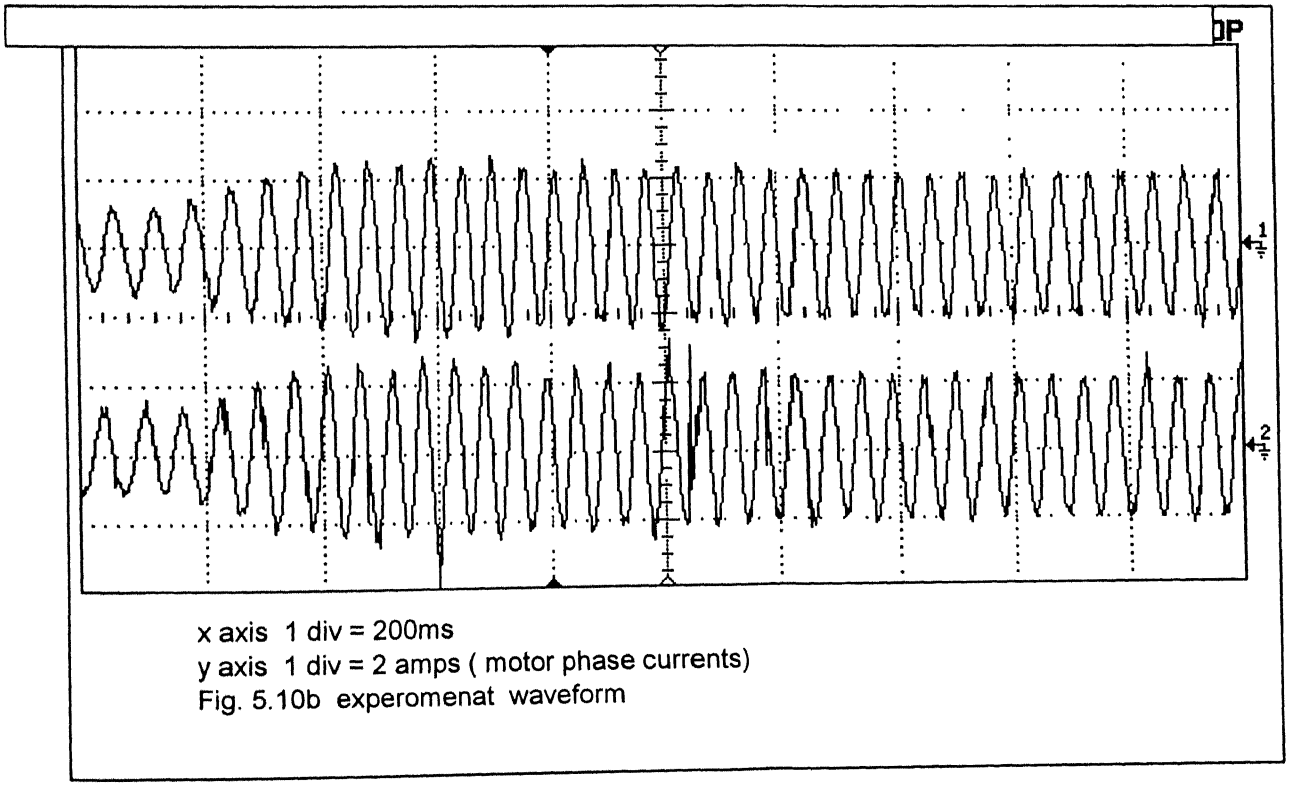

x axis 1 div = 200ms
y axis 1 div = 2 amps (motor phase currents)
Fig. 5.10b experomenat waveform

Fig 5.10 motor phase current during step change of torque

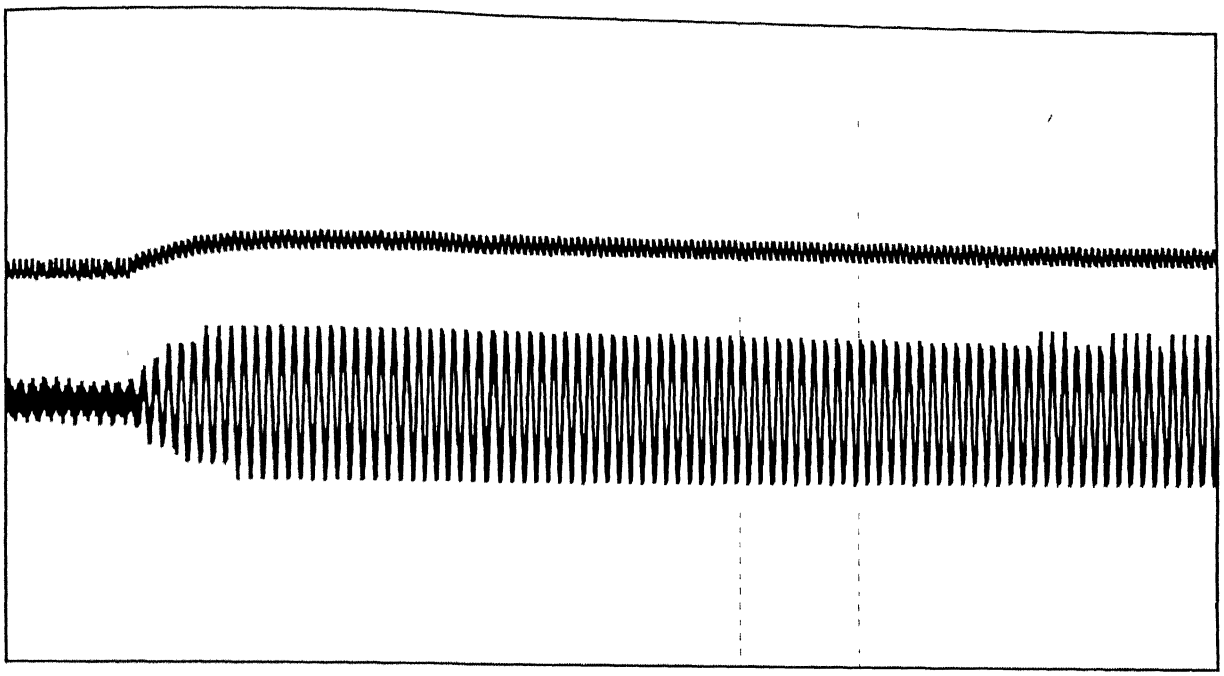

x axis 1div = 200ms (time)
y axis 1div = 1 Nm (torque)
y axis 1div = 4 amps (source current)
Fig 5.11a simulated waveform

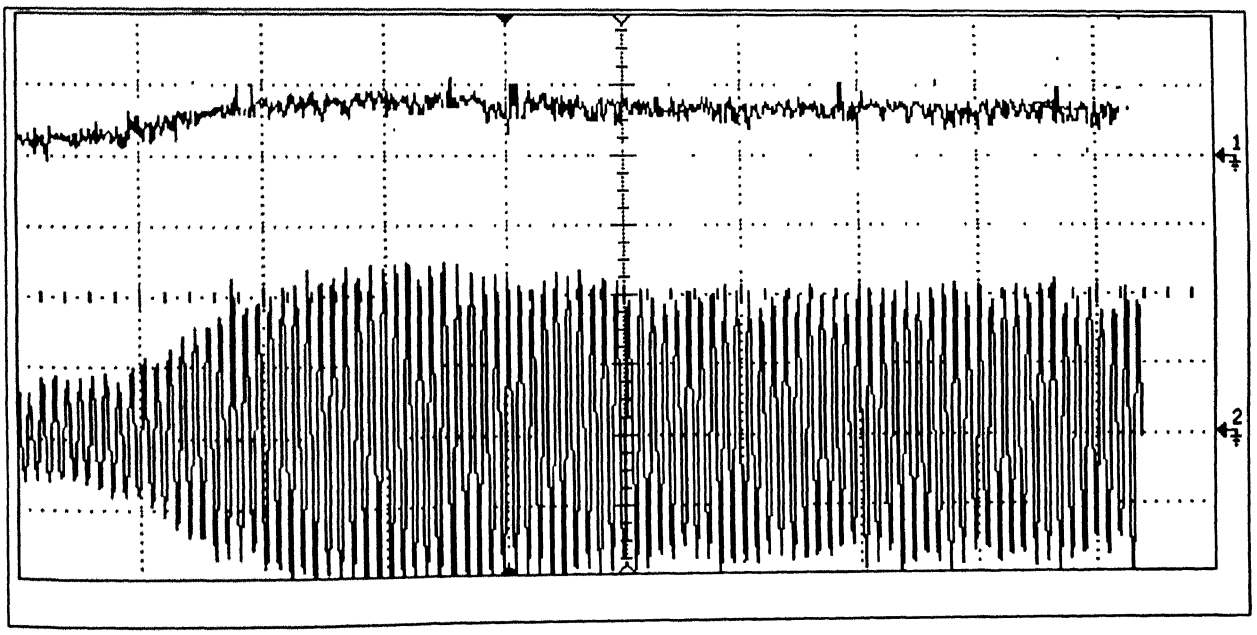

x axis 1div = 200ms (time)
y axis 1div = 2 Nm (torque channel 1)
y axis 1div = 2 amps (source current channel 2)
Fig 5.11b experimental wavefrom waveform

Fig 5.11 torque and source current

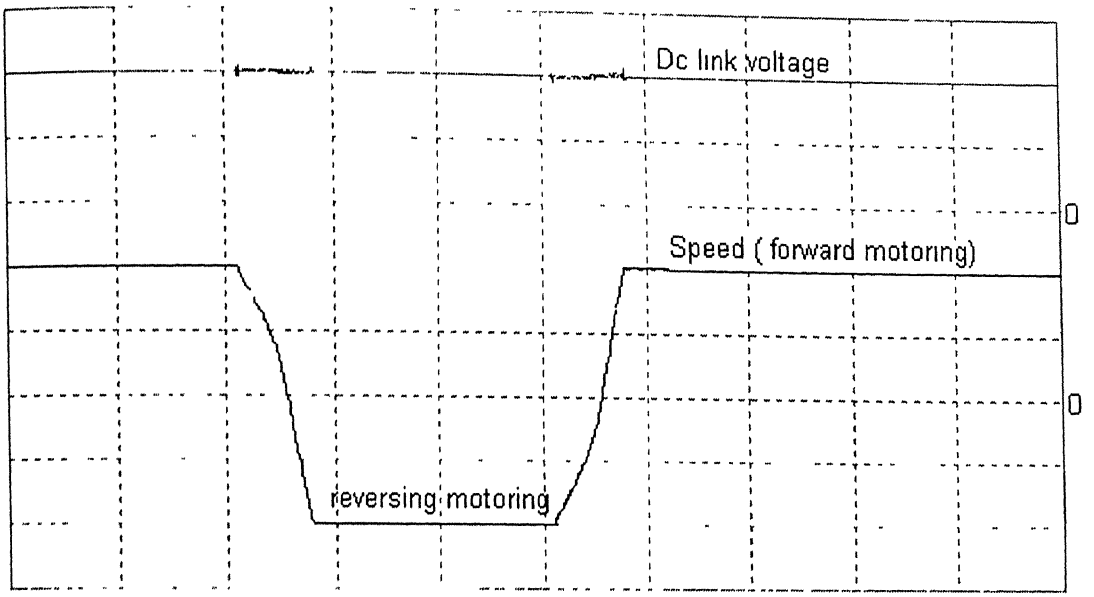

x- axis 1 div = 2 s (time)
y axis 1 div – 50 volts (dc link voltage)
1 div = 250 rpm (motor speed)
Fig 5.12a simulated waveform

x - axis 1 div = 2 s (time)
y - axis 1 div = 50 volts (dc link voltage - Channel 1)
1 div = 250 rpm (motor speed - Channel 2)

Fig. 5.12b Experimental waveform

Fig 5.12 Four quadrant operation of induction motor

Chapter 6

CONCLUSIONS

6.1 Contributions of the Present Thesis Work

The design, simulation and PC-based implementation of four quadrant direct torque and flux control of induction motor has been presented in this thesis. The results show that the harmonics in the source current is less, and power factor is unity. Reversible power is also possible during regenerating mode of the drive. The transient response of the drive is fast with independent control of the flux and the torque. In the transient state, the highest torque response is obtained by selecting the fastest accelerating voltage vector so as to produce the maximum slip frequency. The amplitude of the flux is also controlled to attain the maximum efficiency in steady state operation. Torque response is excellent throughout the entire speed range.

The contribution of the present thesis can, thus, be summarised as follows.

1. Simulation of single phase synchronous link converter.
2. Modeling and simulation of a direct torque and flux controlled induction motor drive system.
3. PC-based implementation of the proposed drive system, and comparison of experimental and simulated results.

6.2 Scope for the Future Work

In the present work hysteresis current controlled scheme is used for the synchronous link converter. For high power applications, hysteresis current control scheme cannot be used. This is due to the switching frequency limitation of high power

devices. Constant frequency pulse width modulated control scheme is suitable for high power applications.

In the proposed scheme, change in machine parameters is not taken into consideration. If this parameter variation is also considered the accuracy of the results can be improved. Thus if an adaptive motor model is taken the problem of change in characteristics with a change in machine parameters can be tackled and results can be improved. The reference torque is generated by using the motor speed signal, which is usually obtained from a mechanical transducer mounted on the rotor shaft. However, this transducer makes the system less robust and reduce the system reliability. In some cases it is difficult to mount the speed sensor on the motor shaft. The new drive system, namely "speed–sensorless control" can be designed to avoid the use of speed sensors.

devices. Constant frequency pulse width modulated control scheme is suitable for high power applications.

In the proposed scheme, change in machine parameters is not taken into consideration. If this parameter variation is also considered the accuracy of the results can be improved. Thus if an adaptive motor model is taken the problem of change in characteristics with a change in machine parameters can be tackled and results can be improved. The reference torque is generated by using the motor speed signal, which is usually obtained from a mechanical transducer mounted on the rotor shaft. However, this transducer makes the system less robust and reduce the system reliability. In some cases it is difficult to mount the speed sensor on the motor shaft. The new drive system, namely "speed–sensorless control" can be designed to avoid the use of speed sensors.

References

[1] T. Kataoka, K. Mizumachi, and S. Miyari, "A pulsewidth controlled ac to dc converters to improve power factor and wave form of ac line current," *IEEE Trans Ind. Appl*, vol. IA –15, pp. 670–675, Nov/Dec. 1979.

[2] H. Zander, "Self–commutated rectifier to improve line conditions," *in Proc. IEEE*, vol –120, No.9, Sept. 1973.

[3] Kocher and Steigerwald, "Ac-to-dc converter with high quality input waveforms," *IEEE Trans. Ind. Appl.*, vol. IA-19, No. 3, July/Aug. 1983, pp. 586-599.

[4] O. Stihi, and B. T. Ooi, "Single phase controlled current rectifier ," *IEEE Trans PE, 3* (PE-4), pp. 453-459, Oct 1988.

[5] E. P. Weichmann, P. D. Ziogas, and V. S. Stefanovic, "A novel bilateral power conversion scheme for variable frequency static power supplies," *IEEE Trans Ind. Appl.*, vol. Ia-21, pp. 1225-1233, Sept./Oct. 1985.

[6] B. T. Ooi, J. E. Dixon, A. B. Kulakarni, and Masahiro Nishimoto "An integrated AC driv system using a controlled –current PWM Rectifier /Inverter link." *IEEE Trans. on power electronics*, vol.3, No.1, Jan. 1988, pp. 64- 70.

[7] T. G. Habetler, "A space vector –based rectifier regulator for ac/dc/ac converters," *IEEE Trans. on power electronics*, vol. 8, No.1, Jan.1993, pp.30 – 36.

[8] F. Blaschke, "The principle of field orientation as applied to the new transvector closed loop control system for rotating field machines," *Siemens review*, vol. 34, pp. 212-220, May 1972.

[9] S.P.Das, "Design, simulation and implementation of a current controlled VSI-fed induction motor with indirect field orientation," *M. Tech. Thesis IIT Kharagpur* 1991.

[10] P. C. Krause, O. Wasynczuk, S. D. Sudhoff, *"Analysis of Electric Machinery,"* *IEEE press New York.*

Appendix A

Specifications of 3 -Phase induction motor

Ratings

Power = 1.1 kW

Voltage = 415 line – line

Current = 2.6 amps

Speed = 1410 rpm

Moment of inertia of motor- generator system = .012kg m^2

Stator parameters

Resistance = 8.2 ohm

Leakage inductance = .026 H

Magnetizing inductance = .0377 H

Rotor parameters

Resistance = 4.3 ohm

Leakage inductance =.026 H

Specifications of dc machine

Ratings:

Power = 1 hp

Voltage = 230 volts;

Current = 4.5 amps

Speed = 1500 rpm

```
/* CALCULATION OF FLUXES AND MOTOR CURRENTS BY USING R-K METHOD */
for(i=0;i<4;++i)
{
Iqs1=(Ls*f_qs1-Lm*f_qr1)/Del;
Iqr1=(Lr*f_qr1-Lm*f_qs1)/Del;
Ids1=(Ls*f_ds1-Lm*f_dr1)/Del;
Idr1=(Lr*f_dr1-Lm*f_ds1)/Del;
      K1[i]=h*(Vqs-Rs*Iqs1);
K2[i]=h*(Vds-Rs*Ids1);
K3[i]=h*(-Rr*Iqr1+Wr*f_dr1);
K4[i]=h*(-Rr*Idr1-Wr*f_qr1);
if(i==0 || i==1)
{
f_qs1+=K1[i]/2.0;
f_ds1+=K2[i]/2.0;
f_qr1+=K3[i]/2.0;
f_dr1+=K4[i]/2.0;
}
if(i==2)
{
f_qs1+=K1[i];
f_ds1+=K2[i];
f_qr1+=K3[i];
f_dr1+=K4[i];
}
}
   f_qs+=(K1[0]+2*(K1[1]+K1[2])+K1[3])/6.0;
   f_ds+=(K2[0]+2*(K2[1]+K2[2])+K2[3])/6.0;
   f_qr+=(K3[0]+2*(K3[1]+K3[2])+K3[3])/6.0;
   f_dr+=(K4[0]+2*(K4[1]+K4[2])+K4[3])/6.0;
   flux_s=sqrt(f_ds*f_ds+f_qs*f_qs);
   f_qs1=f_qs;
   f_ds1=f_ds;
   f_qr1=f_qr;
   f_dr1=f_dr;
   Iqs=(Ls*f_qs-Lm*f_qr)/Del;
     Iqr=(Lr*f_qr-Lm*f_qs)/Del;
     Ids=(Ls*f_ds-Lm*f_dr)/Del;
     Idr=(Lr*f_dr-Lm*f_ds)/Del;
     Irms=sqrt((Ids*Ids+Iqs*Iqs)/2);
   Ia=Ids;
   Ib=-.5*Ids+.866*Iqs;
   Ic=-.5*Ids-.866*Iqs;

   Te=3.0/4.0*P*(f_ds*Iqs-f_qs*Ids);
   ks=h*P/(2*J)*(Te-Tl-2/P*B*Wr);
```

IGBT specifications

Voltage rating = 1200 V

Current rating = 50 A

Specifications of Tachogenerator

Calibration factor = 6 V/1000rpm

Resistance = 20 Ohms

Max speed 2000 rpm

Current sensor specifications

The LEM module LA55-p is a current transducer for electronic measurement of currents with galvonis isolation between the primary (high power) circuit and secondary (low power) circuits.

Sensitivity = .5 V/A

Appendix B

Specifications of the ACL-8112PG Card used for interfacing

Main Features

The ACL-8112PG Enhanced Multi-function Data Acquisition Card provides the following features

1. 16 single ended analog input channels .
2. Two 12-bit monolithic multiplying analog output channels.
3. On-chip sample and hold.
4. 16 digital input channels.
5. 16 digital analog output channels.
6. Programmable sampling rate of up to 100KHz
7. 37-pin D-type connector
8. Three A/D trigger modes : software trigger, programmable trigger and external pulse trigger.
9. Compact size : half-size PCB.

Specifications

Analog input (A/D converter)

Converter	:	successive approximation type
Analog input channels	:	16 single - ended
Resolution	:	12-bit
Input range	:	± 10, ±5, ± 2.5, ±1.25, ±.625
Conversion time	:	8 μs
Over-voltage protection	:	continuous ±35V maximum
Input impedance	:	10MΩ
Data transfer	:	Program control

Accuracy	:	0 015 of reading ± 1bit

Analog output (D/A converter)

Output channels	:	2 double buffered analog Output
Resolution	:	12 –bit
Output range	:	Internal reference 0-5 or 0-10 External reference max. +10 or –10
Converter	:	B.B.DAC7541 or equivalent, monolithic multiplying
Settling time	:	30μs
Linearity	:	± ½ bit
Output driving	:	±5mA

Digital I/O (DIO)

Channel	:	16 TTL compatible inputs and outputs
Input voltage	:	low - Min.0V, Max. 0.8V high - Min. 2V

General specifications

I/O Base address	:	16 consecutive address Locations
Connector	:	37 –pin D-type connector
Operating temperature	:	0 °C - 55 °C
Power consumption	:	+5V , 450mA typical +12V , 120mA typical

Appendix C

1 Simulation Program

```
#include<stdio.h>
#include<math.h>
#define max 10

        /* VARIABLES DECLARATIONS */
int i,j,k,count,count1,count2,sw,sa,sb,sc;
float Vdc,Vao,Vbo,Vco,Va,Vb,Vc,Ia,Ib,Ic,Irms;          /* declaration of voltages and
                                                        currents*/

float K1[4],K2[4],K3[4],K4[4];
float Vds,Vqs,Ids,Iqs,Iqr,Idr,Ids1,Iqs1,Iqr1,Idr1;
float Wrm,Wr,Te,flux_s,flux,flux_r;                    /* declaration of actual values */
float f_qs,f_ds,f_qr,f_dr;                             /* of fluxes,torque speed */
float f_qs1,f_ds1,f_qr1,f_dr1,df_dr,df_qr;             /* of fluxes,torque speed */
float Wref,Wref1,Te_ref,flux_ref;                      /* delcaration of reference speed and
                                                          torques */

float Th1,Th2,Re,t,h,ks,ang,w;
float En,En1,En2,Kp,Ki,Kp1,Ki1,ds,dm,Pm,Il,Tl=0;
float J,B,P,Lm,Lls,Llr,Xls,Xlr,f,Del,Xm,Rs,Rr,Ls,Lr;   /* declaratipn of motor variables */
float Vdcr,Vdc_ref,Lsr,r,Vm,Cd,wr,Is;                  /* declaration of rectier side variables */
float Vs,Id,k1,k2,k3,k4,L1,L2,L3,L4;
float Kr,L,Enr,E1r,E2r,Kpr,Kir,Is_ref,Im;

main()
{
  /* DATA AND VARIABLES INITIALIASATION */

  B=0; J=.012; Rs=8.3; Rr=4; P=4; Ls=.403; Lr=.403; Lm=.377;
  Vm=50; Vdcr=50; Vdc_ref=100; Lsr=.008; Cd=.022; r=.164;
  Flux_ref=.56; Wref=104.56;  Wref1=-104.56;
  Kp=15; Ki=.6; Kpr=.8; Kir=23;
  ang=2*4*atan(1)/3.0;
  h=.00018;
  Del = Ls*Lr - Lm*Lm;
  Wr=Ia=Ib=Ic=0;
  wr=2*4*atan(1)*50.0;
  count1=count2=count=0;
  Th1=E1r=E2r=Enr=0;
        for(t=0; t<4; t+=h)
          {
           if(t>2)
```

```
        {
       if(Wrm<0) Tl=-1.0;
          else
         Tl=1.0;
        }
     if(t>1) Wref=Wref1;
    /* CALCULATION OF REFERENCE TORQUE AND FLUX*/
     En2=Wref-Wr;
         Te_ref=Te_ref+Kp*(En2-En1)+Ki*En1*h;
         En1=En2;
         if(Te>Te_ref+.05)
           dm=-1;
           else
           if(Te<Te_ref-.05)
             dm=1;
             else
               dm=0;
         if(flux_s<=flux_ref-.002)
           ds=1;
           else
            if(flux_s>=flux_ref+.002)
              ds=0;


  /* CALCULATION OF FLUX VECTOR REGION(sector) */
         if(Th1>=330  || Th1<30)
           Re=1;
         if(Th1>=30 && Th1<90)
           Re=2;
         if(Th1>=90 && Th1<150)
           Re=3;
         if(Th1>=150 && Th1<210)
           Re=4;
         if(Th1>=210  && Th1<270)
           Re=5;
         if(Th1>=270 && Th1<330)
            Re=6;
      /* SWTCHING LOGIC SELECTION TABLE */
       if(ds==1)
        {
          if((dm==1  && Re==1) || (dm==-1  && Re==3))
            {
          sa=1;
          sb=1;
          sc=0;
            }
```

```
if((dm==1  && Re==2) || (dm==-1 && Re==4))
  {
sa=0;
sb=1;
sc=0;
  }
if((dm==1  && Re==3) || (dm==-1  && Re==5))
  {
sa=0;
sb=1;
sc=1;
  }
if((dm==1  && Re==4) || (dm==-1 && Re==6))
  {
  sa=0;
  sb=0;
  sc=1;
  }
if((dm==1  && Re==5) || (dm==-1  && Re==1))
  {
sa=1;
sb=0;
sc=1;
  }
if((dm==1  && Re==6) || (dm==-1  && Re==2))
  {
sa=1;
sb=0;
sc=0;
  }
 if(dm==0  && (Re==1 || Re==3 || Re==5))
  {
 sa=1;
 sb=1;
 sc=1;
  }
 if(dm==0  && (Re==2 || Re==4 || Re==6))
  {
 sa=0;
 sb=0;
 sc=0;
  }
}
if(ds==0)
 {
  if((dm==1  && Re==1) || (dm==-1 && Re==5))
```

```
 {
sa=0;
sb=1;
sc=0;
 }
if((dm==1  && Re==2) || (dm==-1 && Re==6))
 {
sa=0;
sb=1;
sc=1;
 }
if((dm==1  && Re==3) || (dm==-1 && Re==1))
 {
sa=0;
sb=0;
sc=1;
 }
if((dm==1  && Re==4) || (dm==-1 && Re==2))
  {
sa=1;
sb=0;
sc=1;
  }
if((dm==1  && Re==5) || (dm==-1 && Re==3))
 {
 sa=1;
 sb=0;
 sc=0;
 }
if((dm==1  && Re==6) || (dm==-1 && Re==4))
 {
sa=1;
sb=1;
sc=0;
 }

 if(dm==0  && (Re==1 || Re==3 || Re==5))
  {
 sa=0;
 sb=0;
 sc=0;
  }
 if(dm==0  && (Re==2 || Re==4  || Re==6))
  {
 sa=1;
 sb=1;
```

```
        sc=1;
         }
      }
/* ------------------------------------------------- */
/*     SYNCHRONOUS LINK CONVERTER CONTROL PART    */
/* -------------------------------------------------*/
   if(count1==0)
       {
       count1=180;
       E2r=Vdc_ref-Vdcr;
       }
        Enr=Enr+Kpr*(E2r-E1r)+Kir*h*E2r;
       count1--;
        E1r=E2r;
        if(Enr>10)
        Enr=10;
        else
        if(Enr<-10)
        Enr=-10;
        Im=Enr;
        Is_ref=Im*sin(wr*t);
        Vs=Vm*sin(wr*t);
        if(Is<=Is_ref-.02 ) sw=1;
        if(Is>Is_ref+.02) sw=-1;
        k1=h*(Vm*sin(wr*t)+sw*Vdcr+sw*r*Is)/Lsr;
        L1=h*(-sw*Is-Il)/Cd;
        k2=h*(Vm*sin(wr*t+h/2.0)+sw*(Vdcr+L1/2.0)+sw*r*(Is+k1/2.0))/Lsr;
        L2=h*(-sw*(Is+k1/2.0)-Il)/Cd;
        k3=h*(Vm*sin(wr*t+h/2.0)+sw*(Vdcr+L2/2.0)+sw*r*(Is*k2/2.0))/Lsr;
        L3=h*(-sw*(Is+k2/2.0)-Il)/Cd;
        k4=h*(Vm*sin(wr*t+h)+sw*(Vdcr+L3)+sw*r*(Is+k3))/Lsr;
        L4=h*(-sw*(Is+k3)-Il)/Cd;
        Kr=(k1+2.0*k2+2.0*k3+k4)/6.0;
        L=(L1+2.0*L2+2.0*L3+L4)/6.0;
        Is=Is+Kr;
        Vdcr=Vdcr+L;
        Vdc=Vdcr;
        Vao=sa*Vdc;
        Vbo=sb*Vdc;
        Vco=sc*Vdc;
    Va=(2*Vao-Vco-Vbo)/3;
    Vb=(2*Vbo-Vao-Vco)/3;
    Vc=(2*Vco-Vao-Vbo)/3;
        Vqs=(Vb-Vc)/1.732;
    Vds=2*(Va-.5*(Vb+Vc))/3.0;
```

```
        Wr=Wr+ks;
        Wrm=2/P*Wr;
        Pm=Te*Wrm+3*Irms*Irms/2*Rs;
        Il=Pm/Vdc;
  if(count==0)
          {
          printf( " %f %f %f %f ", t,Ia,Ib,Ic);
       /*  printf("%f  %f  %f  %f  %f ",t,Wrm*(30/3.1428)/100,Vdcr/20,Is,Vs/10);
          printf(" %f  %f  %f  ",Ia,Ib,Ic);
          printf("  %f  %f  %f  %f  ",Te/10,f_ds,f_qs,flux_s);
      */  printf("\n");
         count=1;
         }

        if(f_ds==0 && f_qs==0)
         Th1=0;
         else
           Th1=atan2(f_qs,f_ds);
           Th2=180*Th1/(4*atan(1));
           if(Th2<0)
            Th2=Th2+360;
           Th1=Th2;
         count=count-1;
      }
    }
```

2 Listing of Real Time PC-based Program

```
#include<stdio.h>
#include<time.h>
#include<conio.h>
#include<dos.h>
#include<math.h>
#define BASE_ADDR 0x300
#define PORT 0x2C0
#define TRUE 1

float    Enr,E1r,E2r;
float    Im,Kpr=.8,Kir=20,Vdc_ref=100,Im1,Im2;
int      sa=0,sb=0,sc=0,Re,P=4;
int      p,val,val1,i,j,k,check,ch,ch1,ch2,cn;
clock_t  start=0,end=0;
float    Vdc,Vao=0,Vbo=0,Vco=0,Va=0,Vb=0,Vc=0,Vn=0,Vqs=0,Vds=0;
float    Ia=0,Ib=0,Ic=0,Iqs=0,Ids=0,Iqr=0,Idr=0,flux,f_qs,f_ds,f_qr,f_dr;
float    Iqr1,Idr1,Ids1,f_qs1,f_ds1,f_qr1,f_dr1;
float    K1[4],K2[4],K3[4],K4[4];
float    Rs=8.0,Rr=4.3,Lls=.026,Llr=.026,Lm=.377,B=0,J=.012,del;
float    Wref=104.0,Wr=0,W=0,Te_ref=0,Te,flux_ref=.56,Tl;
float    Kp=15,Ki=.6,t,h=.00018,Th1,Th2,En1,En2,dm,ds;

main()
     {
    del=(Lls+Lm)*(Lls+Lm)-Lm*Lm;
    outportb(BASE_ADDR+10,0);
     outportb(BASE_ADDR+12,0);
     outportb(BASE_ADDR+11,01);
     outport(BASE_ADDR+5,0);
     outport(BASE_ADDR+4,0);
     start=clock();
     for(t=0;t<=4;t+=h)
       {

            /*  SENSING OF  ANALOG SIGNALS  */

       for(p=0;p<5;p++)
       {
       if(p==3)
       continue;
```

```
j=0;
outportb(BASE_ADDR+10,p);
outportb(BASE_ADDR+12,p);
while(TRUE)
{
val=inportb(BASE_ADDR+5);
check=val;
check &=0x10;
++j;

if(!check)
  break;

  else
  {
   for(i=0;i<10;++i)
   if(j==10)
   {
    printf(" time out on ad conversion \n");
    exit(1);
   }
  }
 }

  val1=inport(BASE_ADDR+4)&0xFF;
  val =((val & 0x0F)*256)+val1;
  val=val-2048;
 if(p==0)
 Ib=(val/2048.0)*5*2;
 if(p==1)
 Ic=(val/2048.0)*5*2;
  if(p==2)
  Vdc=(val/2048.0)*500.0;
  if(p==4)
  Wr=(val/2048.0)*10*34.9/1.3778;
 }

  /*  REFERENCE CURRENT  GENERATOR FOR SYNCHRONOUS LINK
CONVERTER  */
  E2r=Vdc_ref-Vdc;
  Enr=Enr+Kpr*(E2r-E1r)+Kir*h*E2r;
  E1r=E2r;
  if(Enr>10)
  Enr=10;
  if(Enr<-10)
  Enr=-10;
```

```
Im=Enr;
if(Im>=0)
{
Im1=Im;Im2=0;
}
else
{
Im1=0;Im2=-Im;
}
ch=floor((Im2)*4096/30);
ch1=ch/256;
ch2=ch-ch1*256;
outport(BASE_ADDR+4,ch2);
outport(BASE_ADDR+5,ch1);
ch=floor(Im1*4095/30);
ch1=ch/256;
ch2=ch-ch1*256;
outport(BASE_ADDR+6,ch2);
outport(BASE_ADDR+7,ch1);

 /* SENDING SIGNALS OUT */

 ch=floor((4095*(f_ds+1))/5);
 ch1=ch/256;
 ch2=ch-ch1*256;
 outport(PORT+0,ch1);
 outport(PORT+1,ch2);

 ch=floor((4095*(f_qs+1))/5);
 ch1=ch/256;
 ch2=ch-ch1*256;
 outport(PORT+2,ch1);
 outport(PORT+3,ch2);
  if(t>=2)
 {
  Wref=-104;
  Kpr=.05;
  Kir=10;
  Kp=100;
  Ki=.005;
  }

  Vao=sa*Vdc;
  Vbo=sb*Vdc;
  Vco=sc*Vdc;
  Vn=(Vao+Vbo+Vco)/3.0;
```

```
Va=Vao-Vn;
Vb=Vbo-Vn;
Vc=Vco-Vn;
Vds=(Va-.5*(Vb+Vc))*2/3.0;
Vqs=(.866*(Vb-Vc))*2/3.0;
Ia=-(Ic+Ib);
Ids=(Ia-.5*(Ib+Ic))*2/3.0;
Iqs=(.866*(Ib-Ic))*2/3.0;

/*   CALCULATION OF  D-AXIS AND Q AXIS FLUXES  BY USING R-K 4TH
ORDER METHOD  */
for(i=0;i<4;++i)
{
Iqr1=((Lls+Lm)*f_qr1-Lm*f_qs1)/del;
Idr1=((Lls+Lm)*f_dr1-Lm*f_ds1)/del;
K1[i]=(Vqs-Rs*Iqs)*h;
K2[i]=(Vds-Rs*Ids)*h;
K3[i]=(-Rr*Iqr1-(W-Wr)*f_dr1)*h;
K4[i]=(-Rr*Idr1+(W-Wr)*f_qr1)*h;
if((i==0) || (i==1))
  {
  f_qs1+=K1[i]/2.0;
  f_ds1+=K2[i]/2.0;
  f_qr1+=K3[i]/2.0;
  f_dr1+=K4[i]/2.0;
  }
 if(i==2)
  {
   f_qs1+=K1[i];
   f_ds1+=K2[i];
   f_qr1+=K3[i];
   f_dr1+=K4[i];
  }
 }
   f_qs+=(K1[0]+(K1[1]+K1[2])*2+K1[3])/6.0;
   f_ds+=(K2[0]+(K2[1]+K2[2])*2+K2[3])/6.0;
   f_qr+=(K3[0]+(K3[1]+K3[2])*2+K3[3])/6.0;
   f_dr+=(K4[0]+(K4[1]+K4[2])*2+K4[3])/6.0;

   Iqr=((Lls+Lm)*f_qr-Lm*f_qs)/del;
   Idr=((Lls+Lm)*f_dr-Lm*f_ds)/del;
   f_qs1=f_qs;
   f_ds1=f_ds;
   f_qr1=f_qr;
   f_dr1=f_dr;
   Te=3*P*(f_ds*Iqs-f_qs*Ids)/4.0;
```

```
flux=sqrt(f_qs*f_qs+f_ds*f_ds);

if(f_ds==0 && f_qs==0)
  Th1=0;
  else
       Th1=atan2(f_qs,f_ds);
       Th2=180*Th1/(4*atan(1));
       if(Th2<0)
       Th2+=360;
       Th1=Th2;
/*  REFERENCE TORQUE  GENERATOR  */
       En2=Wref-Wr;
       Te_ref+=Kp*(En2-En1)+Ki*En2*h;

       En1=En2;
       if(Te>Te_ref+.0005)
        dm=-1;
       else
       if(Te<Te_ref-.0005)
        dm=1;
       else
        dm=0;
       if(flux<flux_ref-.0002)
        ds=1;
       else
       ds=0;
      /* CALCULATION OF FLUX VECTOR REGION(sector) */

      if(Th1>=330 || Th1<30)
        Re=1;
      if(Th1>=30 && Th1<90)
        Re=2;
      if(Th1>=90 && Th1<150)
        Re=3;
      if(Th1>=150 && Th1<210)
        Re=4;
      if(Th1>=210  && Th1<270)
        Re=5;
      if(Th1>=270 && Th1<330)
        Re=6;

/* SWTCHING LOGIC SELECTION TABLE */

if(ds==1)
 {
   if((dm==1  && Re==1) || (dm==-1  && Re==3))
```

```
    {
sa=1;
sb=1;
sc=0;
    }
if((dm==1  && Re==2) || (dm==-1 && Re==4))
    {
sa=0;
sb=1;
sc=0;
    }
if((dm==1  && Re==3) || (dm==-1  && Re==5))
    {
sa=0;
sb=1;
sc=1;
    }
if((dm==1  && Re==4) || (dm==-1 && Re==6))
    {
    sa=0;
    sb=0;
    sc=1;
    }
if((dm==1  && Re==5) || (dm==-1  && Re==1))
    {
sa=1;
sb=0;
sc=1;
    }
if((dm==1  && Re==6) || (dm==-1  && Re==2))
    {
sa=1;
sb=0;
sc=0;
    }
if(dm==0  && (Re==1 || Re==3 || Re==5))
    {
sa=1;
sb=1;
sc=1;
    }
if(dm==0  && (Re==2 || Re==4 || Re==6))
    {
sa=0;
sb=0;
sc=0;
```

```
        }
    }
if(ds==0)
    {
    if((dm==1  && Re==1) || (dm==-1 && Re==5))
        {
    sa=0;
    sb=1;
    sc=0;
        }
    if((dm==1  && Re==2) || (dm==-1 && Re==6))
        {
    sa=0;
    sb=1;
    sc=1;
        }
    if((dm==1  && Re==3) || (dm==-1 && Re==1))
        {
    sa=0;
    sb=0;
    sc=1;
        }
    if((dm==1  && Re==4) || (dm==-1 && Re==2))
        {
    sa=1;
    sb=0;
    sc=1;
        }
    if((dm==1  && Re==5) || (dm==-1 && Re==3))
        {
       sa=1;
       sb=0;
       sc=0;
        }
    if((dm==1  && Re==6) || (dm==-1 && Re==4))
        {
    sa=1;
    sb=1;
    sc=0;
        }

    if(dm==0 && (Re==1 || Re==3 || Re==5))
        {
    sa=0;
    sb=0;
    sc=0;
```

```
        }
    if(dm==0  && (Re==2 || Re==4  || Re==6))
        {
    sa=1;
    sb=1;
    sc=1;
        }
  }
/*  SENDING THE CONTROL SIGNALS TO HARDWARE */

cn=4*sc+2*sb+sa;
switch(cn)
    {
    case 0:
    outport(BASE_ADDR+13,0x00);
    break;
    case 1:
    outport(BASE_ADDR+13,0x01);
    break;
    case 2:
    outport(BASE_ADDR+13,0x02);
    break;
    case 3:
    outport(BASE_ADDR+13,0x03);
    break;
    case 4:
    outport(BASE_ADDR+13,0x04);
    break;
    case 5:
    outport(BASE_ADDR+13,0x05);
    break;
    case 6:
    outport(BASE_ADDR+13,0x06);
    break;
    case 7:
    outport(BASE_ADDR+13,0x07);
    break;
  }
}
end=clock();
printf("  time= %f    \n ",(end-start)/CLK_TCK);
}
```

2.2.2 Selection of DC link Voltage

When an SLC is used as the front end converter in variables speed drives, the dc link voltage is decided by the line-to-line voltage rating of the motor. The anti-parallel feedback diodes in SLC have to be normally reverse biased to ensure that switching of the devices can control the waveform of ac input current. This requires the dc link voltage V_{dc} to be always greater than peak of ac voltage [4].

$$V_{dc} \geq \sqrt{2}. V_s$$

Hence the motor voltage rating, the dc link voltage and the input ac voltage should be properly matched in a variable speed drive.

2.2.3 Selection of synchronous link inductor

If synchronous link inductor is large, the rate of rise and fall of current is small. Hence the response is slow. But if the inductance is small then the source current harmonics increase. So proper value of inductance should be used for fast response and low harmonics in the source current.

2.2.4 Selection of DC link capacitor

The main criterion for selecting the dc link capacitor C_d is based on the allowable ripple in the dc link. It is a usual practice to limit the ripple voltage due to second harmonic currents within the 5% of the rated value of dc link voltage. As the output of the dc link is fed to the inverter, effective measures have to be taken to limit the effect of second harmonic component. The value capacitor is given by the expression [16].

$$C_d \geq (V_s\ I_{s1}\ 100)\ /(2\ w V_{dc}^2\ x\ )$$

Where x is % of ripple in the dc link voltage,

I_{s1} is fundamental component of source current.